Marine Geology 431 (2021) 106372

Contents lists available at ScienceDirect

Marine Geology

journal homepage: www.elsevier.com/locate/margo

Mid-to-late Holocene upper slope contourite deposits off Capo Vaticano (Mediterranean Sea): High-resolution record of contourite cyclicity, bottom current variability and sandy facies

Eleonora Martorelli [a,*], Alessandro Bosman [a], Daniele Casalbore [a], Francesco Chiocci [b], Aida Maria Conte [a], Letizia Di Bella [b], Gemma Ercilla [c], Federico Falcini [d], Pierpaolo Falco [e], Virgilio Frezza [b], Giovanni Gaglianone [b], Biagio Giaccio [a], Marco Mancini [a]

[a] CNR, IGAG, Italy
[b] SAPIENZA, Università di Roma, Italy
[c] CSIC, ICM, Spain
[d] CNR, ISMAR, Italy
[e] Università Parthenope, Italy

ARTICLE INFO

Keywords:
Sandy contourites
Bi-gradational sequences
Holocene
Moat
m-Levantine Intermediate Water

ABSTRACT

The upper continental slope offshore Capo Vaticano (southern Tyrrhenian Sea) is characterized by a contourite depositional system with well-developed elongated sediment drifts. This system is related to a northward paleo-bottom current, similar to the present-day modified-Levantine Intermediate Water (modified-LIW) flowing from the Messina Strait. In this work, we show results from an integrated analysis of descriptive oceanography, high-resolution seismic profiles and core data (i.e., grain size, foraminiferal assemblages, tephrostratigraphy and AMS radiocarbon dating) collected from the crest and moat sectors of drift deposits. The studied succession formed since the mid Holocene, under the action of the modified-LIW and the stratigraphic architecture indicates an upslope migration of the moat and rather stable position of the crest sector. Grain-size features recorded from two sediment cores indicate the occurrence of a succession of complete bi-gradational sand-rich contourite sequences. Sandy facies were observed both as lag deposits formed in active moat channel and as coarser intervals of bi-gradational sequences forming drift deposits close to its crest. Their occurrence would highlight that upper slope environments impacted by intermediate water masses and proximal to sandy sources may represent favorable settings for accumulation of sandy sediment. The moat sector is characterized by a more complex stratigraphic record, where either moat sedimentation or lateral deposition of finer sediment occur, suggesting that further investigation is required to better understand this complex element of contourite systems. Based on available age information, some of the bi-gradational sequences probably formed during the Dark Age Cold Period, providing example of a small-scale cyclicity of contourite deposition, likely related to short-term (possibly multicentennial scale) fluctuations of the paleo modified-LIW. According to age constraints and analysis of foraminiferal assemblages, these fluctuations were likely governed by climate variations, with a weaker activity during warmer periods and faster currents during colder events.

1. Introduction

Contourites are defined as sediments deposited or substantially reworked by the persistent action of bottom currents (Stow et al., 2002a; Rebesco et al., 2014). Over the last decades, studies concerning the analysis of contourite deposits and along-slope processes increased significantly, highlighting their importance, among other, for depositional processes shaping continental margins and abyssal plains (Stow et al., 2002a; Rebesco et al., 2014; Hernández-Molina et al., 2016; Mosher et al., 2017; Thiéblemont et al., 2019). Recent studies concerning contourites highlighted the need for a better understanding of oceanographic and sedimentary processes governing their formation, as well as for robust diagnostic criteria for deciphering contourite facies (e.g., Rebesco et al., 2014; Hernández-Molina et al., 2016; Yin et al., 2019).

* Corresponding author.
E-mail address: eleonora.martorelli@cnr.it (E. Martorelli).

https://doi.org/10.1016/j.margeo.2020.106372
Received 4 November 2019; Received in revised form 14 October 2020; Accepted 16 October 2020
Available online 6 November 2020

This is particularly true for sandy deposits that are relatively uncommon in the geological record and still poorly known, if compared with their fine-grained counterpart (Brackenridge et al., 2018). According to Brackenridge et al. (2018) and Stow and Smillie (2020), sandy contourites can occur either as part of the bi-gradational sequence (i.e., the coarsest division of the contourite facies model) in mud-rich drifts or as distinct sandy units in sand sheets, oceanic gateways, contourite channels and terraces. However, further studies are needed to provide their systematic classification and to establish a precise relation between the nature of the deposit, bottom current dynamic and other associated oceanographic processes (Hernández-Molina et al., 2016; Miramontes et al., 2020; Stow and Smillie, 2020). A further main interest in the study of contourites is related to the possibility to decipher paleoceanographic and paleoclimate changes, as these deposits represent long-term archives that provide key information on ocean circulation and past climate (e.g., Knutz, 2008). In various seas worldwide, studies concerning contourites revealed major oceanographic changes and allowed reconstruction of past climatic variability over a broad range of time scales, including the late Quaternary (e.g., Llave et al., 2006; Voelker et al., 2006; Toucanne et al., 2007, 2012; Frigola et al., 2008; Knutz, 2008; Bahr et al., 2014; Hanebuth et al., 2015; Lebreiro et al., 2018). In the Mediterranean, there is still little knowledge on the link between thermohaline circulation and late Quaternary-Holocene short-term (sub-millenial-timescale) climate variability (e.g., Cacho et al., 2001). Very high-resolution stratigraphic records can bridge this gap, in particular for the past few millennia, that are most relevant to the uniqueness of modern climate variability (Jones and Mann, 2004).

The upper continental slope off Capo Vaticano (south-eastern Tyrrhenian Sea) provides an expanded stratigraphic record of postglacial contourite deposits (maximum thickness of about 25 ms two way travel time - TWT), with a high potential to investigate variability of contourite sedimentation in both time and space. The studied deposits belong to a small contourite system characterized by well-developed elongated drifts formed during the late Quaternary (Martorelli et al., 2016). Here, the formation of contourites and associated erosive elements has been related to the action of bottom currents, likely similar to the present-day modified-Levantine Intermediate Water (modified-LIW), flowing from the Messina Strait. In this work, we analyze for the first time contourite sedimentation during the Middle-Late Holocene, focusing on sedimentary facies developed on an elongated drift, and on bottom current variability recorded by complete bi-gradational contourite sequences. The main objectives are: (1) to outline the main textural features of the contourite deposits, including sand-rich facies; (2) to decipher variability of sedimentation across the crest and moat sectors of elongated sediment drift deposits, using sedimentological and seismic information; (3) to decipher rapid fluctuations of bottom currents, discussing the possible influence of climate variations on bottom current variability and development of complete bi-gradational sequences, using sedimentological, foraminiferal and geochronological information.

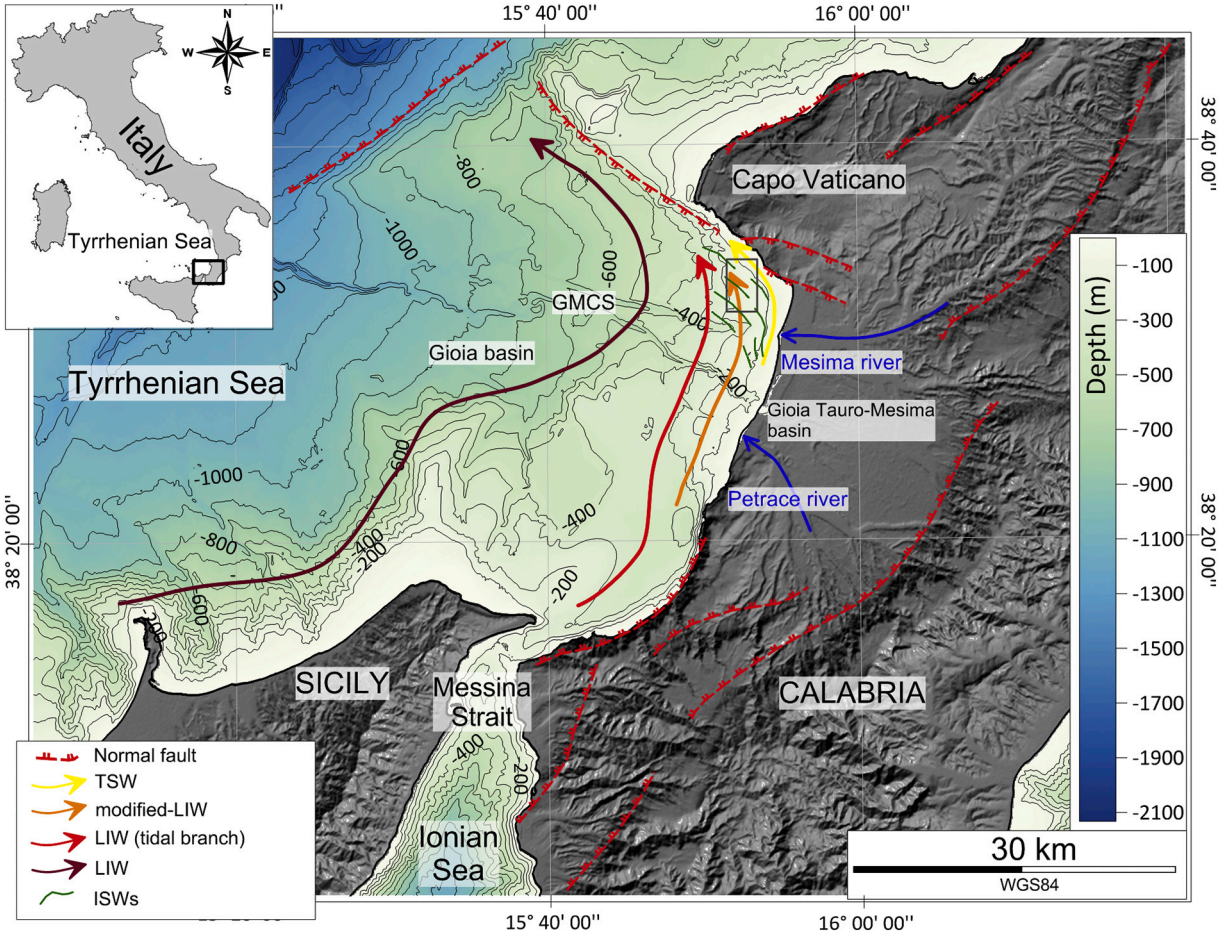

Fig. 1. Study area with indication of main water masses. TSW: Tyrrhenian Surface Water; LIW: Levantine Intermediate Water; modified-LIW: modified Levantine Intermediate Water. GMCS: Gioia-Mesima canyon-channel system. Grey rectangle: study area. Green lines: sea surface expression of internal solitary waves (ISWs) from SAR roughness-Sentinel1 image of May 10, 2019 (ESA-OceanDataLab). (For interpretation of the references to colour in this figure legend, the reader is referred to the web version of this article.)

2. Study area

2.1. Geological context

The Calabro-Tyrrhenian margin (Fig. 1) is a Neogene rifted margin, formed during the opening of the Tyrrhenian Sea, along the westward side of the Calabrian Arc (Sartori, 2003). Post-orogenic extensional tectonics that influenced the Calabrian Arc determined: its fragmentation in highs (e.g., the Coastal Range and Capo Vaticano Promontory) and basins (e.g., the Gioia Tauro-Mesima basin; Fig. 1), high rates of tectonic uplift during the Quaternary (Antonioli et al., 2006) and strong seismicity (CPTI Working Group, 2004). High-energy water courses dissect the mainland with high discharge of sediment. The main ones are the Mesima and Petrace rivers, which deliver high volume of sediment to the shelf (Pierdomenico et al., 2016). The study area is characterized by a narrow shelf and a steep upper continental slope (Fabbri et al., 1980) with a complex morphology mainly determined by canyons, channels, landslides, contourite drifts and moats (Figs. 1 and 2; Martorelli et al., 2016). The main morphological feature of the shelf-slope sector is the Gioia-Mesima canyon-channel system (GMCS in Fig. 1), which dissects the seafloor, starting from the coastal sector and running down to −1700 m (Colantoni et al., 1992; Bosman et al., 2017; Casalbore et al., 2018). During the Holocene, the area has been affected by tephra deposition events produced by wide explosive eruptions of the Aeolian Arc and from the peri-Tyrrhenian magmatic provinces (e.g., Campanian Province and Sicily Province). The main tephra layer is related to the 79 CE Pompei eruption of Somma-Vesuvius (Zanchetta et al., 2011) that is characterized by a large dispersal, including the Ionian and Tyrrhenian seas and the Gulf of S. Eufemia located NE of Capo Vaticano (Cosentino et al., 2017).

Offshore Capo Vaticano, a northward oriented bottom current possibly related to a water mass similar to the present-day modified-LIW formed small-scale (a few tens of km long and a few km wide) contourite deposits, between 90 and 300 m water depth (Fig. 2; Martorelli et al., 2016).

2.2. Oceanographic features

The main water masses circulating offshore Capo Vaticano are: the Tyrrhenian Surface Water (TSW) and the Levantine Intermediate Water (LIW); a third water mass is often recognized in between the TSW and the LIW, named modified-LIW (Fig. 1; Marullo and Santoleri, 1986; Hopkins, 1988; Povero et al., 1990; Sparnocchia et al., 1999). The TSW is a branch of the Atlantic surface water and is characterized by a temperature of ~14–20 °C and a salinity of ~38.0. Tidal, amphidromic effects, acting at the sill region of the Strait of Messina, give rise to a semi-diurnal northward flux (named "*rema montante*"; from Marullo and Santoleri, 1986; Fig. 1) of the LIW (~14.2 °C and a salinity of ~38.8),

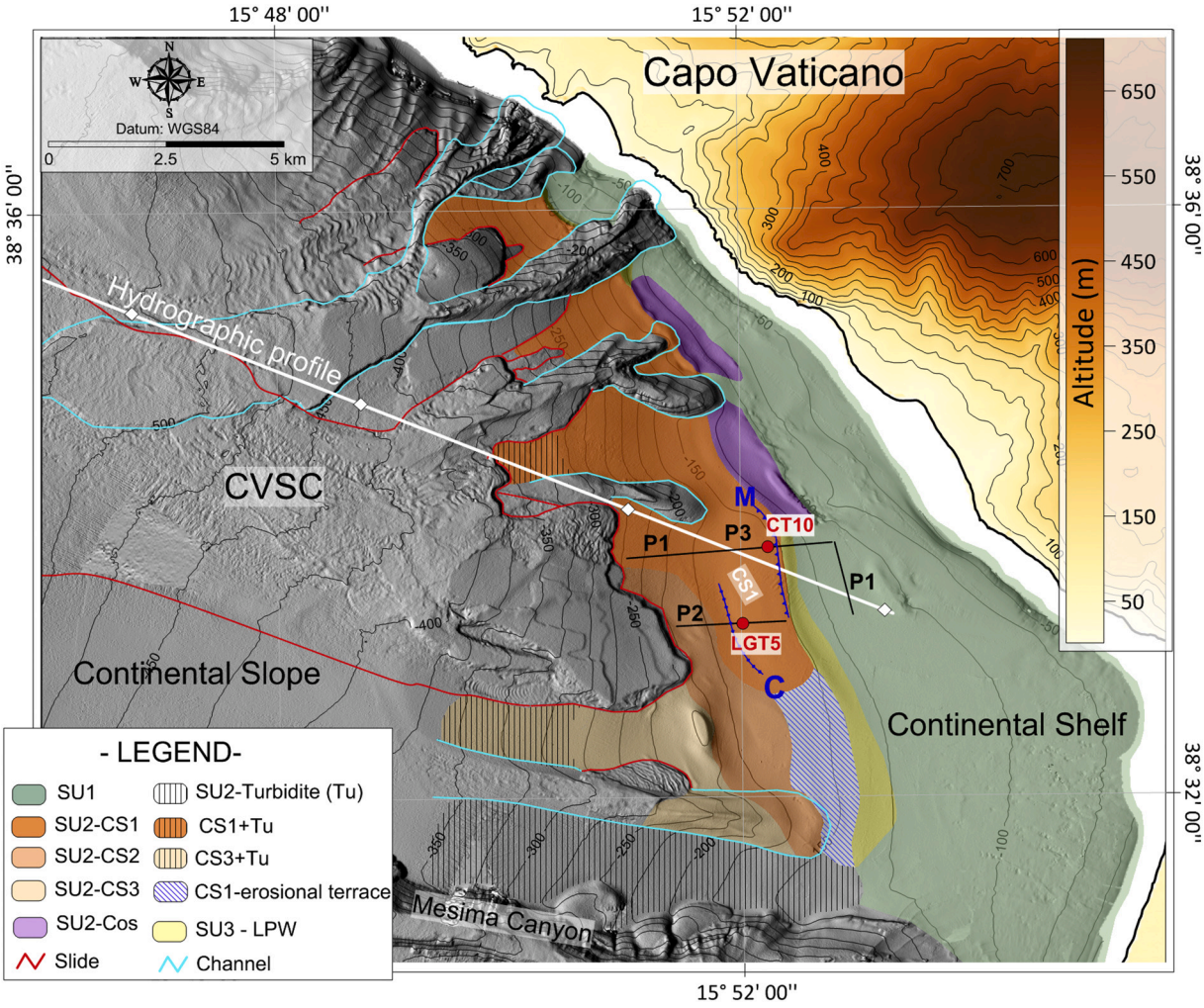

Fig. 2. Shaded relief map of multibeam bathymetry of the southern sector of Capo Vaticano with indication of contourite drifts and location of the two sediment cores (red circles), seismic profiles P1, P2 and P3 (black lines) and hydrographic profile (white line)-stations (white rhombuses). C: crest of the CS1 drift; M: moat of the CS1 drift. SU1-3: seismic units: CS1-3: elongated drifts; Cos: shelf drift; LPW: lowstand prograding wedge. Coordinate system: UTM WGS 84-33 North (modified from Martorelli et al., 2016). (For interpretation of the references to colour in this figure legend, the reader is referred to the web version of this article.)

coming from the Ionian basin and issuing from the sill of the Messina Strait (Hopkins et al., 1984; Lascaratos et al., 1999; Robinson et al., 2001; Droghei et al., 2016); once in the Tyrrhenian basin, the tidal branch of LIW that debouches from the Messina Strait flows geostrophically northward, along the Calabrian margin. The modified-LIW is a salty vein (38.5, T of ~14.3 °C), flowing geostrophically northward, in between the TSW and the tidal branch of LIW. The origin of this modified-LIW was hypothesized by Marullo and Santoleri (1986) as the result of mixing processes, occurring at the sill region during the "*rema montante*", as well as resulting from the breaking of internal solitary waves (La Forgia et al., 2018; Cavaliere et al., 2020). These particular non-linear internal waves (i.e., solitons) are one of the most peculiar features of the area: they generate at the Strait of Messina due to the hydraulic jump occurring during the strong tidal forcing and propagate northward at the interface between the LIW and the TSW, reaching the frontal slope of Capo Vaticano (Fig. 1), where they likely break, giving rise to strong mixing and intense bottom shear stress (Alpers and Salusti, 1983; Marullo and Santoleri, 1986; Brandt et al., 1999; La Forgia et al., 2018; Cavaliere et al., 2020). The main branch of LIW, coming from the Sicily Channel, is located offshore from the area occupied by the modified-LIW and the tidal branch of LIW (Fig. 1).

3. Data and methods

3.1. Oceanographic data

CTD (Conductivity-Temperature-Depth), LADCP (Lowered Acoustic Doppler Current Profiler) and beam attenuation data were collected during the TyGraF cruise (Urania R/V) in 2013. In particular, the instrumentation we used was: a Sea-Bird SBE 911; a LADCP (Lowered ADCP) system that employed two Teledyne RDI Workhorse 300-kHz ADCP, installed as a down- and up-looker; a Sea-Bird C-Star Transmissometer for measuring beam transmittance at 650 nm. All instruments were installed on a CTD rosette system and lowered down to the bottom to obtain the profile of the full water column; all vertical profiles were re-binned in bins of 1 m length to allow for intercomparison. The hydrographic investigation focused on the detection and characterization of the alongshore currents flowing between 100 and 700 m depth by means of seven cross-shore transects and a finer sampling between 100 and 300 m depth (Fig. 3). The survey strategy was based on the oceanographic setting reported by Marullo and Santoleri (1986), Hopkins (1988), Povero et al. (1990) and Sparnocchia et al. (1999), which describe in detail the formation and vertical distribution of TSW, TDW, LIW, and modified-LIW. CTD cast distribution were aimed at capturing the sub-mesoscale hydrographic pattern of the basin, as well as mixing processes due to the breaking of the internal solitary waves that are supposed to occur over the frontal slope of Capo Vaticano (Marullo and Santoleri, 1986). LADCP data were used to verify and quantify the geostrophic and ageostrophic flows, associated with the observed water masses. In this study, we consider and analyze the hydrographic transect that runs along the southern sector of Capo Vaticano and it is formed by 5 equally spaced vertical profiles (white rhombuses in Fig. 2).

3.2. Sub-bottom profiles

Sub-bottom profiles were collected during the MAGIC-IGAG cruise in 2011 (Minerva1 R/V, CNR, Italy). The Sub Bottom Profiler Benthos

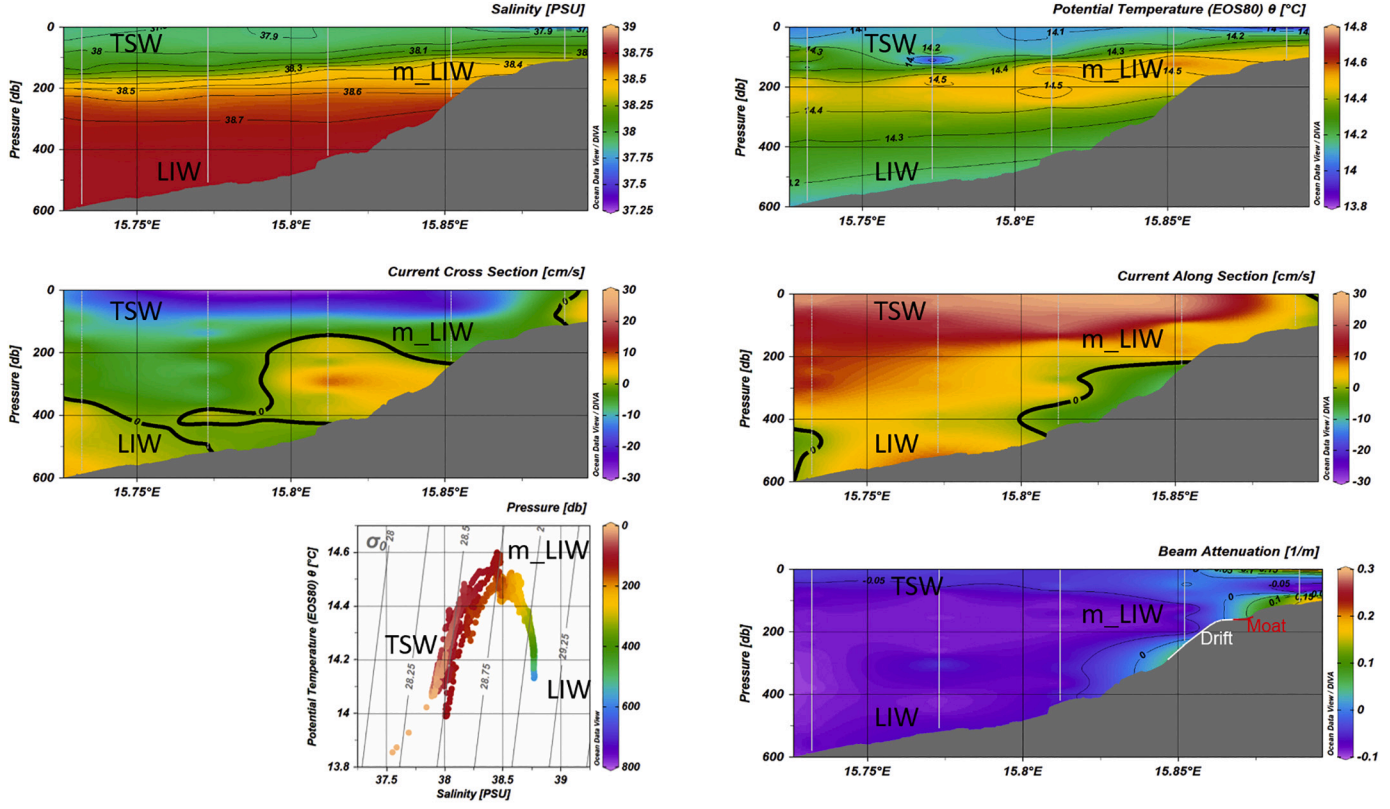

Fig. 3. Hydrographic vertical cross sections of hydrographic profile T5 (see Fig. 2 for location), showing temperature, salinity, beam attenuation, and current velocity (cross-section and along-section) south of Capo Vaticano (February, 2013). Both temperature and salinity patterns show the presence of the three main water masses that acts in this sector, i.e., the Tyrrhenian Surface Water (TSW), the Levantine Intermediate Water (LIW), and the modified Levantine Intermediate Water (m_LIW). Cross and along sections show the strong action of the northward flowing m_LIW near the bottom, where the alongshore velocity is ~8 cm/s and the beam attenuation indicates sediment resuspension in between 100 and 300 m depth. The CS1 drift and moat sectors are indicated in the beam attenuation cross section. (For interpretation of the references to colour in this figure legend, the reader is referred to the web version of this article).

Chirp III (2–7 kHz) was used to investigate the shallow subsurface using a ping rate of 0.5 s. Post-processing of seismic lines was performed with GeoSuite All works software to increase the amplitude of seismic signal through automatic gain control and time varying gain. Data interpretation was conducted using Kingdom Suite software. An acoustic velocity of 1500 m/s was used for time–depth conversion for both water and sediment. Max. vertical resolution is ca. 30 cm. Data positioning was provided by a differential GPS.

3.3. Sediment cores and analysis

3.3.1. Core retrieving and sedimentological analysis

Two gravity cores were collected during the TyGraF cruise (core CT10; Urania R/V, 2013) and the LGT-Gioia77 Eurofleet cruise (core LGT5; Minerva1 R/V, 2016), at 153 m and 157 m water depth (Table 1), from the crest and moat sectors (Fig. 2). The cores are 2.3 m and 3.55 m long and recovered the uppermost part of drift deposits. The two cores were sampled for grain size and foraminiferal analyses (88 collected samples) with variable spacing, ranging from 10 cm (in the homogeneous muddy intervals) to 2–5 cm (in the sandy intervals). Four samples (two per core) were collected for AMS radiocarbon dating and two samples were analyzed for tephra analysis. The sedimentary structures were examined through visual description of cores. The grain size analyses were performed at Sapienza University of Roma, on bulk sediment and using the Sympatec Helos laser diffraction particle size analyzer for the fine-grained fraction (from 0.5 to 62 μm) and sieves for the coarse-grained fraction (> 62 μm). A combination of laser diffraction and sieving method was used due to occurrence of sediment with variable grain size, generally including coarse sediment and great amount of muddy sediment. In order to reduce the risk of under-representativeness for coarser populations of laser diffraction analyses, laser diffraction was used for grain size determination of fractions finer than 62 μm. Textural statistical parameters (mean, standard deviation, skewness, kurtosis) were calculated using the Folk and Ward (1957) geometric method (Gradistat software). Sorting, skewness and kurtosis were described using a scheme modified from Folk and Ward (1957) where the statistical parameters terms relate to a metric scale (see table IIe reported in Blott and Pye, 2001). Negative skewness values indicate an excess of fines and has been named “fine skewed”.

3.3.2. Foraminiferal analysis

The samples were used for the foraminiferal analysis in order to characterize paleoclimatic and paleoenvironmental evolution of the succession recovered by the cores CT10 and LGT5. Qualitative and quantitative analyses were conducted on sediment fraction >88 μm and <500 μm. The 88 μm lower limit was set to exclude juvenile specimens (e.g., Lirer et al., 2013; Margaritelli et al., 2016). Each sediment sample was split by a microsplitter into small portions as the material was abundant. In all samples, 250–300 benthic and planktonic foraminifera with well-preserved tests were counted and picked, respectively. Benthic foraminifera were classified according to Loeblich and Tappan (1987), Cimerman and Langer (1991), Sgarrella and Moncharmont-Zei (1993) and World Register of Marine Species (WoRMS; http://www.marinespecies.org); planktonic foraminifera were classified according to Kennet and Snivrasan (1983), Hemleben et al. (1989) and Iaccarino et al. (2007). In order to compare our data with the bio and chronostratigraphical literature data (Lirer et al., 2013; Vallefuoco et al., 2012), the following planktonic grouping was adopted: the *Globigerinoides ruber* group that includes *G. ruber pink* and *G. elongatus*; the *Globigerinoides quadrilobatus* that includes *G. trilobus* and *G. sacculifer*; the *Globigerina bulloides* that includes *G. falconensis*; the *Globigerinella* spp. includes *G. siphonifera* and *G. calida;* and the *Neogobloquadrina* spp. that includes *N. pachyderma, N. incompta* and *N. dutertrei*. Left and right coiling of *Globorotalia inflata* and *G. truncatulinoides* were distinguished and counted separately. In order to characterize the water mass, herbivorous-opportunistic planktonic species (*T. quinqueloba, G. glutinata, G. bulloides*) and carnivorous ones (*G. ruber, G. quadrilobatus, O. universa, Globigerinella* spp.) were considered (Margaritelli et al., 2016). Moreover, on the base of literature data two groups, called for simplicity warm and cold-water group, were identified. They include species not directly influenced by temperature, but mostly occurring associated with the typical temperature markers. The cold group includes: *Turborotalita quinqueloba*, *Globigerinita glutinata*, *Globorotalia scitula*, *Neogloboquadrina incompta*. The warm group includes taxa like *Globigerinoides* spp. (*G. ruber*, *G. trilobus*, *G. quadrilobatus*), *Globigerinella siphonifera* and *Orbulina universa* (Cita et al., 1977; Thunell and Reynolds, 1984; Hemleben et al., 1989; Rohling et al., 1993; Pujol and Vergnaud-Grazzini, 1995). An evaluation of broken, reworked and bad preserved tests was carried out. Both planktonic and benthic foraminiferal species were plotted in percentage values and the relative benthos/plankton ratio (B/P) was calculated. This study adopted the eco-biostratigraphic schemes of Lirer et al. (2013) and Margaritelli et al. (2016), because they offer a complete high-resolution framework for the SE Tyrrhenian Sea during the Late Quaternary.

Table 1
Position, water depth and length of the studied sediment cores.

Gravity core	Latitude	Longitude	Core length (m)	Water depth (m)
CT10	38°33′40.8″	15°52′15.3″	2.3	153
LGT5	38°33′10.6″	15°51′56.4″	3.55	157

3.3.3. Tephra layers

Two cryptotephra, i.e., invisible to the naked eye, were identified during the microscope analysis of the core sediments from core LGT5 at the depths of 299–300 and 169–170 cm below sea floor (bsf). The glass-pumice fraction of the two cryptotephra, labeled CT1 and CT2, was handpicked and selected grains were mounted on epoxy resin for petrographic and chemical analysis. The morphological and textural features of the micropumices and qualitative chemical analyses were carried out under a binocular microscope and through a scanning electron microscopy. Back-scattered-electron images (BSE) and energy-dispersive X-ray (EDS) spectra were determined using a FEI-Quanta 400 (SEM–EDAX) at the Earth Science Department, Sapienza University of Rome (Italy). The grains were then individually analyzed for major elements at the IGAG-CNR (Rome, Italy) using a Cameca SX50 electron microprobe equipped with a five-wavelength dispersive spectrometer. Operating conditions were set to 15 kV accelerating voltage; 15 nA beam current; 10–15 μm beam diameter; 20 s per element counting time. A 10 μm defocused beam was used for glass analyses to minimize volatilization of sodium. Full matrix correction was based on a PAP procedure (Pouchou and Pichoir, 1991).

3.3.4. AMS radiocarbon dating

Four samples were collected for AMS radiocarbon dating analyses (Table 2). Radiocarbon analyses were performed at Beta Analytic Lab, using AMS-standard procedures and chemical pretreatments (acid washes and acid-alkali-acid method; https://www.radiocarbon.com/beta-lab.htm). The four radiocarbon dating were obtained from samples at 164 and 230 cm bsf in core CT10 and from samples at 248 and 354 cm bsf in core LGT5. The four samples were selected in order to have age constraint of the bottom of the cored succession (samples LGT5-354 and CT10-230) and to constrain the age of the coarser divisions of contourite sequences (samples LGT5-248 and CT10-164). Although, muddy intervals would have been more suitable to perform radiocarbon dating, they were not considered because difficulties in separating the finer-grained C1-C5 divisions of two contourite sequences. One sample was obtained from a plant remain (remain of marine phanerogams) recovered within the sediment and three from organic material extracted from bulk samples. The use of the bulk organic matter has been preferred over foraminifera due to the low abundance and fragmented nature of individual planktonic foraminifera species. Calibration of radiocarbon age

Table 2
14C-AMS radiocarbon data obtained for the sediment cores.

Sample name	Depth bsf (cm)	Laboratory code	Analyzed material	$\delta^{13}C$ (‰)	^{14}C age (year BP)	Cal Age (year BP)
CT10_164	164	Beta-499850	Organic sediment	−24.5	1320 +/− 30	1298–1228*
CT10_230	230	Beta-499849	Organic sediment	−23.6	5180 ±30	5991–5905*
LGT5_248	248	Beta-499848	Plant material	−12.9	1850 ±30	1336–1446**
LGT5_354	354	Beta-499847	Organic sediment	−24.1	3630 ±30	3994–3854*

* INTCAL13 database.
** MARINE13 database.

to calendar years has been performed using BetaCal 3.21 (Ramsey, 2009) and INTCAL13 database (Reimer et al., 2013). Sample LGT_248 has been calibrated using the MARINE 13 dataset (Reimer et al., 2013).

4. Results

4.1. Physical oceanography

Hydrographic data (Temperature-Salinity diagrams and the cross-shore vertical hydrographic transects in Fig. 3) show the TSW filling the entire surface layer until ~200 m depth; according to the winter season, the TSW results to be characterized by T ~ 14.2 °C and S ~ 38.0 (Fig. 3; Hopkins, 1988; Povero et al., 1990; Sparnocchia et al., 1999). Below the TSW, we recognize the presence of the tidal branch of LIW (T ~ 14.2 °C and S ~ 38.8), issued directly from the Ionian Sea through the Messina Strait. This water mass is observed to flow geostrophically in the study area, from 250 m depth to the bottom (LIW in Fig. 3). Approaching Capo Vaticano, we also observe a shoreward thickening of the interface that separates the TSW and the LIW (the yellow layer around 200 m depth, visible in both T and S vertical sections of Fig. 3), which reaches a thickness of ~100 m at the eastern side of the transect. We identify this water mass, from 150 to 250 m depth, as the modified-LIW (T ~ 14.5 °C and S ~ 38.5; Fig. 3), which flows along isobaths over the CS1 drift. According to previous literature, this water mass shows higher temperature and lower salinity with respect to the LIW. The shoreward increase of thickness of this layer strongly suggests an enhancement of TSW-LIW mixing nearby the intersection between the TSW-LIW interface and the sea bottom; this is, likely induced by breaking of internal solitary waves that generate at the Strait (Marullo and Santoleri, 1986; La Forgia et al., 2018; Cavaliere et al., 2020). Accordingly, beam attenuation data indicates an increase in near-bottom water turbidity, likely due to sediment resuspension, along the bathymetric level between 100 and 300 m depth (Fig. 3). Near-bottom LADCP measurements show maximum alongshore velocity of ~8 cm/s over the CS1 drift (Fig. 3). All hydrographic parameters we analyzed show, in general, a good correspondence between the bathymetric level over which the modified-LIW interacts with the seafloor and the location of the study contourite drift, i.e., approximately 150–250 m depth (Fig. 3).

4.2. Seismic stratigraphy

The shallow subsurface of the study area is characterized by 3 seismic units (SU1, SU2 and SU3, Figs. 2 and 4) that correspond to those described by Martorelli et al. (2016). Seismic unit SU1 consists of shelf deposits bounded by the seafloor at their top and by an erosive surface at their base (i.e., the Last Glacial Maximum unconformity; LGM-U in Fig. 4). Unit SU2 includes both turbidites (mostly confined to the northern levee of the Mesima Canyon; Fig. 2) and contourites that form different elongated drifts (CS1, CS2, CS3 and Cos in Fig. 2). Unit SU2 is bounded at its base by the ES surface (Figs. 4 and 5). This surface is erosional in many profiles crossing the contourite drifts, down to about 300 ms TWT, and is likely correlated to the LGM unconformity observed on the shelf sector. Seismic unit SU3 consists of a lowstand wedge-shaped prograding deposit (Figs. 2 and 4). More in detail, Chirp profiles across contourite drifts show that unit SU2 can be subdivided in 5 subunits (Figs. 4, and 5), generally a few meters thick (ca. max. 10 m). These subunits are characterized by distinct seismic facies and separated

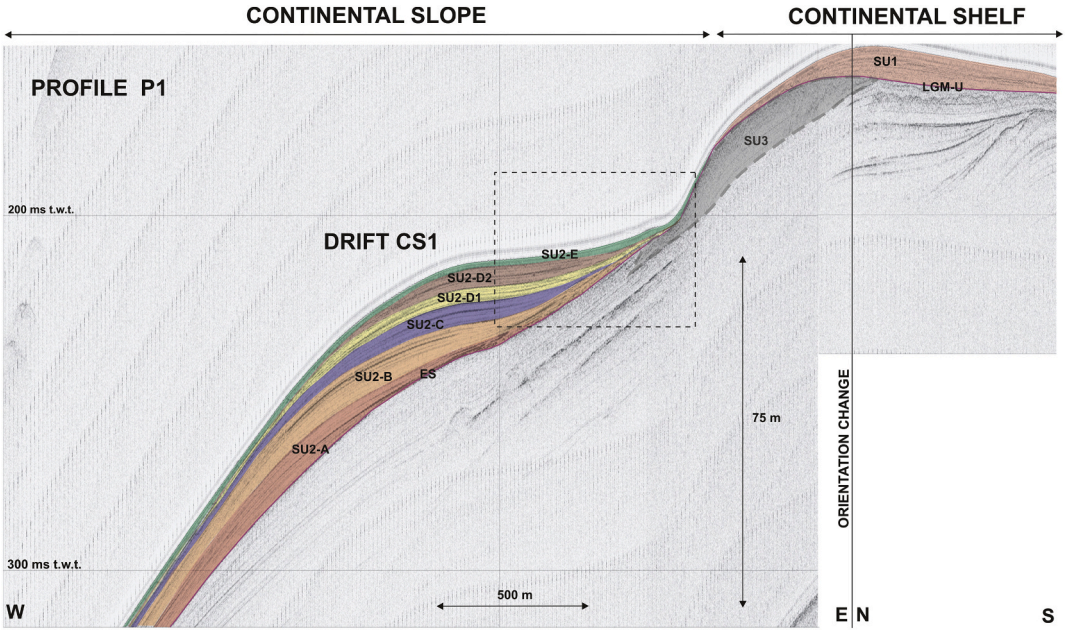

Fig. 4. Interpreted Chirp seismic profile P1 showing seismic units (SU1, SU2 and SU3) identified in the study area and main seismic subunits identified within Unit SU2. See Fig. 2 for location of P1 seismic profile. The dashed rectangle indicates profile P3 shown in Fig. 5.

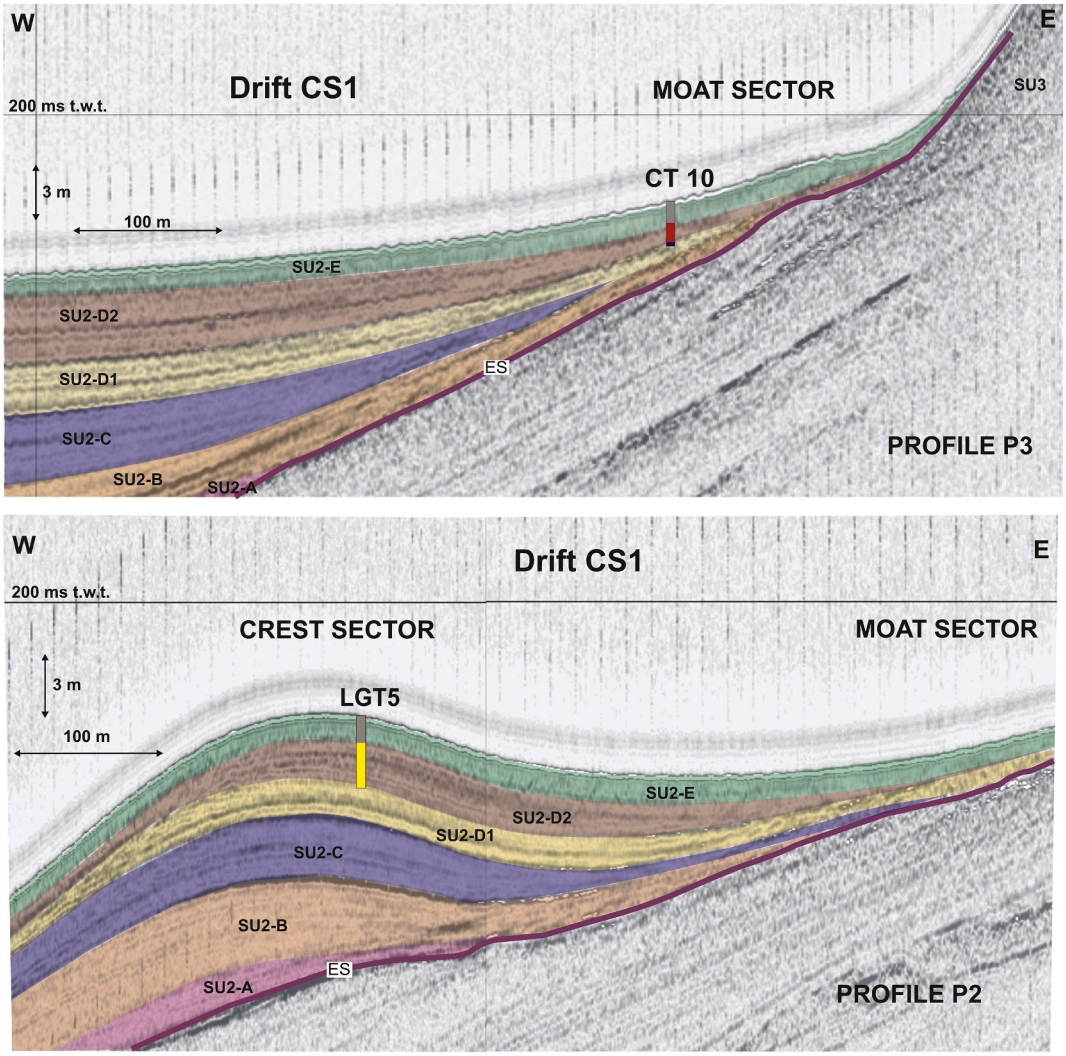

Fig. 5. Seismic subunits identified within Unit SU2 across drift CS1; upper panel Chirp seismic profile P3 across core CT10; lower panel Chirp seismic profile P2 across core LGT5 (see Fig. 2 for location of P2 and P3 seismic profiles). Moat erosion can be recognized within the different subunits forming drift CS1, with an upslope migration through time. The location of the cores with indication of the lithological units is also indicated (Unit 1: blue rectangle; sub-unit 2a: yellow rectangle; sub-unit 2b: red rectangle; Unit 3: grey rectangle). (For interpretation of the references to colour in this figure legend, the reader is referred to the web version of this article.)

by non-depositional or erosional surfaces. Minor non-depositional or erosional surfaces are also present within the subunits. From the bottom to the top the subunits are:

- subunit SU2-A, characterized by moderate amplitude and high-continuity reflectors;
- subunit SU2-B, characterized by moderate amplitude and high-continuity reflectors;
- subunit SU2-C, characterized by a few high-amplitude and high-continuity reflectors;
- subunit SU2-D, characterized by a few high-amplitude and high-continuity reflectors in the lower portion (SU2-D1) and by several high-amplitude and high-continuity reflectors in the upper portion (SU2-D2).
- subunit SU2-E, characterized by a semitransparent facies. This unit drapes both drift CS1 and CS2 with minor changes in thickness; locally (e.g. the erosional terrace, the shelf break sector and some moat areas) it can be absent or very thin.

4.3. *Core lithology and grain size features*

In general, both cores show a dominance of silt and variable sand content, with values between 7 and 50% in core CT10 and between 10 and 53% in core LGT5 (Fig. 6); clay content varies between 7 and 29%. The composition of the sand fraction >88 μm is mostly siliciclastic. Sediment distribution is generally polymodal with a fine tail in both the cores (Fig. ESM1). In the lower part of core CT10, sediment distribution is characterized also by a coarse-grained tail (Figs. 6 and ESM1).

4.3.1. *Lithological units*

Based on grain size data, colour and sedimentary structures, three distinct lithological units (units 1, 2 and 3) can be recognized in the cores; unit 2 was differentiated in two sub-units (2a and 2b) due to differences in grain size (Fig. 6). From the bottom upwards these are:

Unit 1 (11 cm thick; basal part of core CT10: 220–231 cm core depth; Figs. 6, 7 and ESM2a): dark olive to olive grey, silty sand with scattered lithic clasts ranging in size from coarse sand to pebbles 0.5 cm across (Fig. 7). The upper contact is irregular. The dominant mode values are in the coarse silt-sand range (e.g., 62–1414 μm, Table ESM1). The max. Sand content is 50%, the D50 min. is 69 μm (very fine sand) and the D50

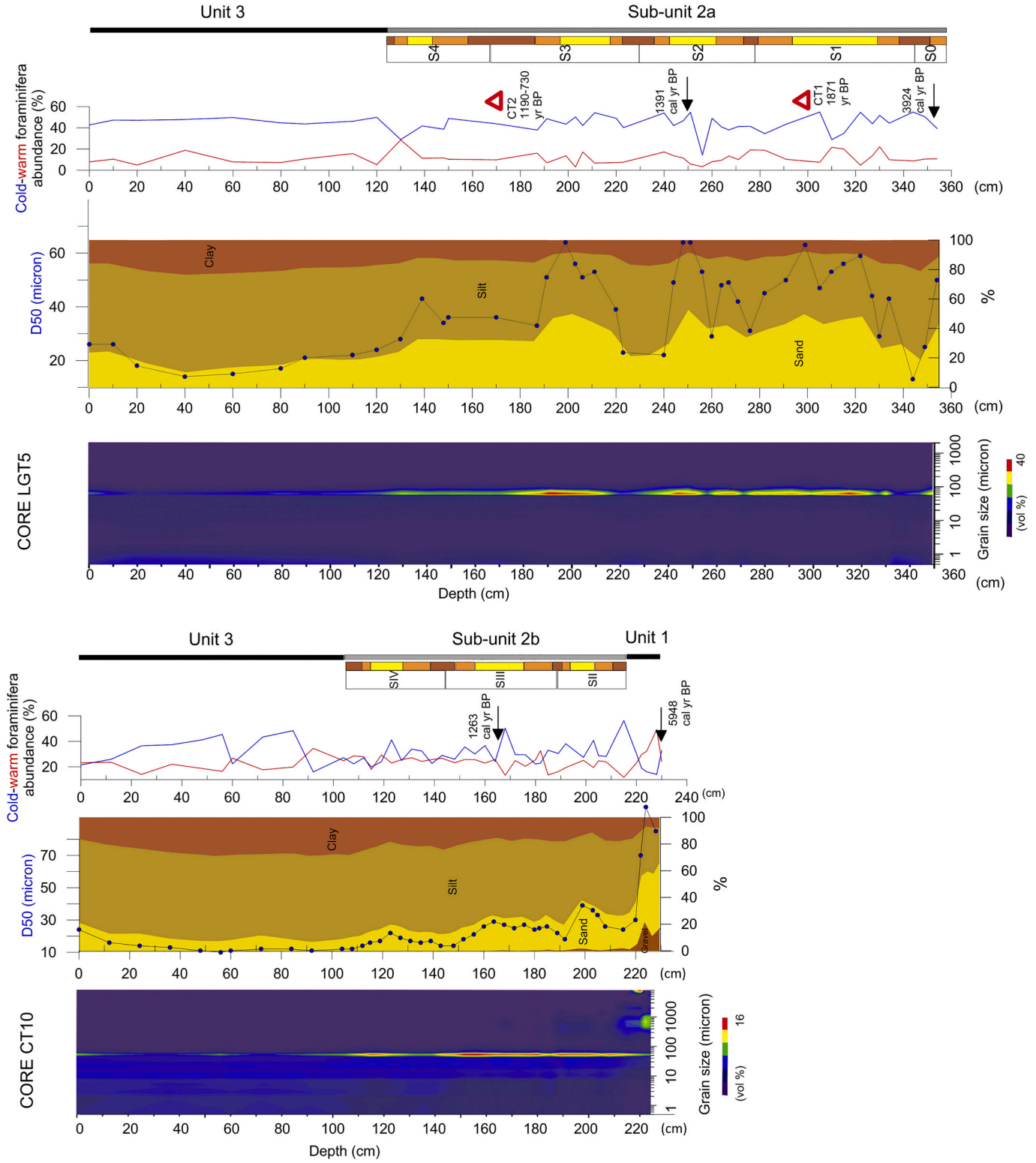

Fig. 6. Grain size and abundance of cold and warm groups of foraminifera along cores CT10 and LGT5. Lithological units (units 1 to 3), bi-gradational sequences (S0 to S4 and SII to SIV) and C1 to C5 divisions (yellow rectangles indicate C3 divisions; orange rectangles indicate C2 and C4 divisions; brown rectangles indicate C1 and C5 divisions) identified within the cores are also indicated. Red triangles indicate tephra CT1 and CT2. Black arrows indicate 14C radiocarbon dates. (For interpretation of the references to colour in this figure legend, the reader is referred to the web version of this article.)

max. is 314 μm (medium sand). In the upper part this unit is fining upward. Sediment is very poorly sorted (10−12) and characterized by negative to positive skewness and platykurtic distribution (Figs. 8, ESM2b and Table ESM1).

Sub-unit 2a (225 cm thick; core LGT5: 130–355 cm core depth): alternating homogenous olive grey sandy silt (finer-grained intervals) and dark olive grey sandy silt and silty sand (coarser-grained intervals); locally the coarser-grained intervals have a mottled appearance (Fig.

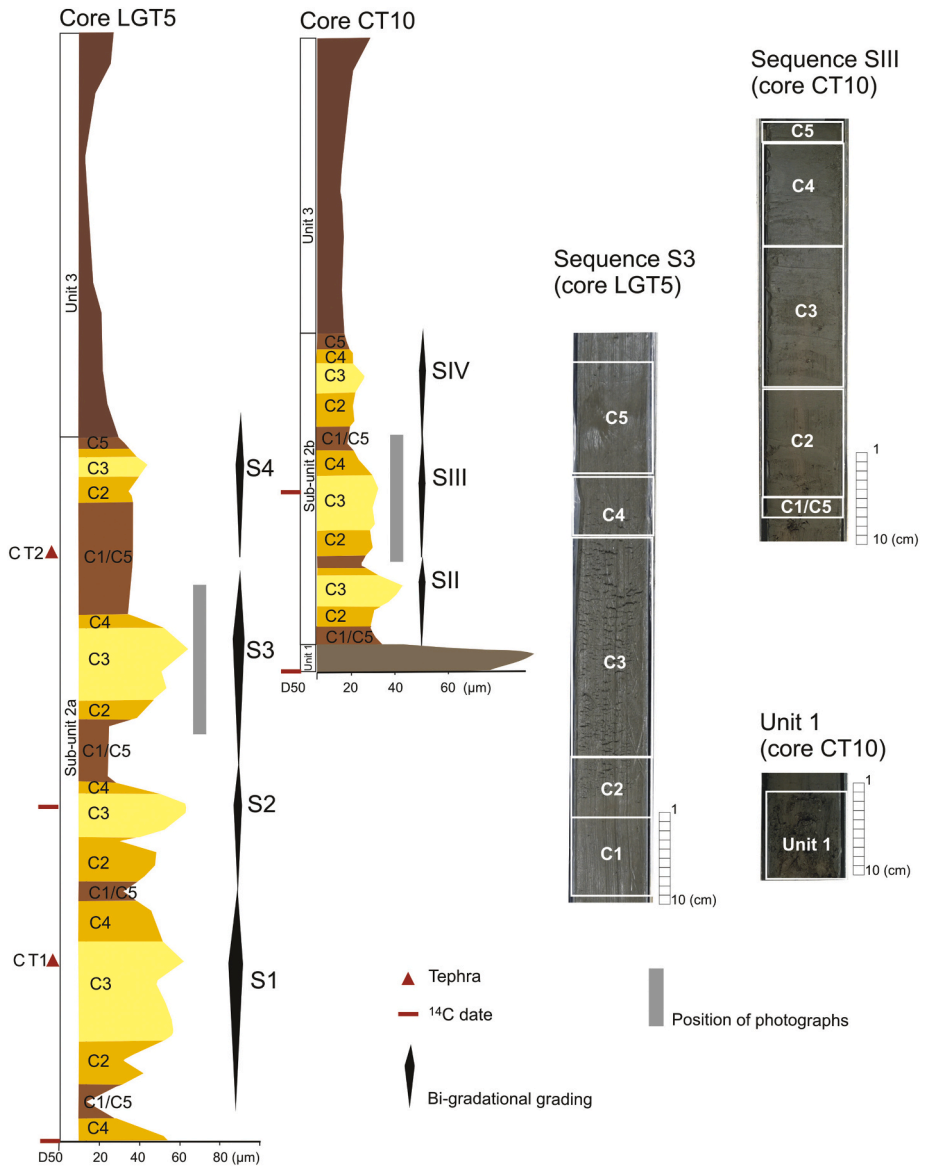

Fig. 7. Contourite sequences identified in the Capo Vaticano sediment cores, with indication of contourite divisions C1 to C5, and detail of core photographs of Unit 1 (core CT10), sequence S3 (core LGT5) and SIII (core CT10). Grey rectangles indicate the position of core photographs. Position of cryptotephras and ^{14}C dates are also indicated.

ESM2a). Upper and lower contacts are gradational. The dominant mode values are in the coarse silt range (62 μm, Fig. ESM1). Finer-grained intervals have a max. Sand content of 31%, whereas the coarser-grained intervals have a max. Sand content of 53%, and are generally composed of small pockets and irregular fine layers (laminae). Finer and coarser-grained intervals are arranged in three main sedimentary sequences (S1, S2 and S3 in Figs. 6 and 7) characterized by a bi-gradational grading (fine to coarse sediment followed by coarse to fine sediment). Possible further bi-gradational sequence are the S4 sequence (Fig. 6), though not so well developed as S1, S2 and S3, and part of a sequence that is present at the base of the core (S0). In the bi-gradational sequences, D50 values range between 13 and 23 and 63–64 μm (S1, S2 and S3), whereas D50 values range between 34 and 43 μm in the S4 sequence (Table ESM1). The sequences are characterized by poorly sorted to very poorly sorted (3–4.5) sediment and negative skewness (−0.7 to −0.1). Kurtosis varies between platykurtic and leptokurtic (0.8–1.4; Fig. ESM2b and Table ESM1). Coarser-grained intervals are better sorted than finer-grained ones and sediment distribution is more negatively skewed. Kurtosis values vary from platykurtic/mesokurtic (finer-grained intervals) to leptokurtic (coarser-grained intervals) (Figs. 8 and ESM2b).

Sub-unit 2b: (111 cm thick; CT10: 108–219 cm core depth): dark olive grey sandy silt fine layers or pockets and subordinate thin finer-grained intervals; locally the coarser-grained intervals have a mottled appearance. Upper and lower contacts are gradational. The dominant mode values are in the coarse silt range (62 μm, Fig. ESM1). Finer-grained intervals have a max. Sand content of 30%. Coarser-grained intervals are very poorly sorted and have a max. Sand content of 36%. Within this unit, three sedimentary sequences with a bi-gradational trend can be distinguished (SII, SIII and SIV in Figs. 6 and 7). These sequences have D50 values ranging between: 14–18 and 22–39 μm, and sediment is very poorly sorted (4.2–7.6), fine skewed or symmetrical and kurtosis varies between platykurtic and leptokurtic (0.9–1.4; Table ESM1). Coarser-grained intervals of sequences SII and SIII are generally characterized by a decrease of sorting and are more leptokurtic than finer-grained intervals. In sequence SIV, kurtosis and sorting are relatively constant whereas skewness slightly decreases in coarser-grained intervals (Fig. 8 and ESM2b).

Unit 3 (108–130 cm thick; upper part of cores CT10 (0–108 cm) and LGT5 (0–130 cm): olive grey homogeneous silt and sandy silt, except for the upper yellowish brown 1 cm, possibly representing an oxidized layer

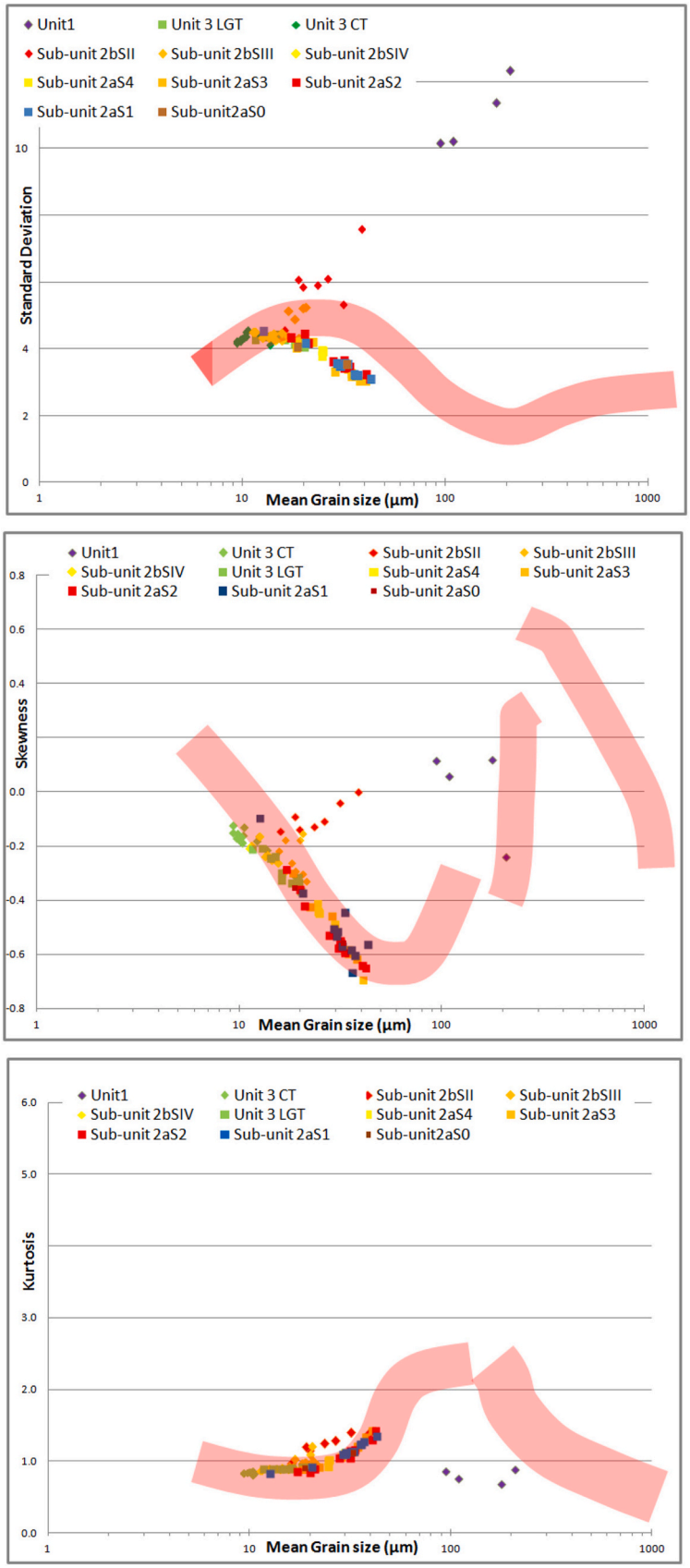

Fig. 8. Cross-plots of mean size against sorting (upper panel), skewness (middle panel) and kurtosis (lower panel) for lithological units and contourite sequences of cores CT10 and LGT5. The reddish areas indicate the grain size trend observed on contourite deposits of the Gulf of Cadiz (derived from Brackenridge et al., 2018).

(Fig. ESM2a). The dominant mode values are in the coarse silt range (62 μm, Fig. ESM1).The max. Sand content is 25%. D50 varies between 10 and 28 μm (Fig. 6). Sediment is very poorly sorted (4–4.6) and sediment distribution is generally platykurtic (ca. 0.8–0.9) and fine skewed (−0.1 to-0.4) (Fig. 8 and ESM2b, Table ESM1).

4.4. Benthic and planktonic foraminifera assemblages

Microfaunal results were described following the subdivision in lithological units indicated in Section 4.3, to better constrain the sedimentary processes and stratigraphic events. A more detailed description is reported in figures ESM3 and ESM4. Broken/reworked tests of benthic and planktonic foraminifera are always present along the cores and, in some samples, they are abundant or very abundant. Nevertheless, the fluctuations of their abundance are not clearly linked to grainsize variations.

4.4.1. Benthic assemblages (Fig. ESM3)

Unit 1: is characterized by the dominance of *Cassidulina* spp. (*Cassidulina crassa,* 12.25%; *Cassidulina carinata,* 13.20%) and *Globocassidulina subglobosa* (12.45%). Significant values (about 13% in total) of typical infralittoral (*Elphidium* spp., *Lobatula lobatula, Quinqueloculina seminulum, Ammonia beccarii*) species are also recorded. The benthic fraction dominates the planktonic one (the mean B/P ratio is 1.50).

Sub-unit 2a: *C. carinata*, *V. bradyana* and *G. subglobosa* are the most abundant species in all sequences, though significant fluctuations. The benthic fraction is generally subordinate to the planktonic one.

Sub-unit 2b: though significant fluctuations, the qualitative compositional content of the benthic foraminiferal assemblages is similar to that observed in Unit 1. A slight increase of agglutinated taxa, such as *Textularia bocki* is evidenced in SIII (6.16%). The B/P ratio increases from SII (1.41) to SIV (1.91).

Unit 3: in core CT10, *B. spathulata* (10.41%), *C. carinata* (37.37%) and *B. marginata* (7.89%) increase significantly while *V. bradyana* shows similar values about 12.40% in respect of the previous units. In core LGT5, this unit is characterized by the dominance of *C. carinata* (18.81%) and *V. bradyana* (14.09%). In both the cores the B/P ratio is mostly >1.

4.4.2. Planktonic assemblages (Fig. ESM4)

Unit 1: plankton is mainly represented by *Globigerina bulloides* (18.36%), *Globigerinoides ruber* (16.64%), *G. quadrilobatus* (12.61%) and *Turborotalita quinqueloba* (11.06%).

Sub-unit 2a: though some significant quantitative fluctuations, in all sequences *T. quinqueloba* (about 30%) and *G. bulloides* (about 24%) dominate.

Sub-unit 2b: *T. quinqueloba* (18.93%), *G. bulloides* (17.87%) and *G. glutinata* (13.20%) dominate in all sequences. In sequence SIV, the increase of *G. ruber* (11.37%) is observed.

Unit 3: in core CT10 *G. bulloides* (21.65%) and *T. quinqueloba* (18.36%) increase significantly and dominate together with *G. glutinata* (10.07%). In core LGT5, Unit 3 is characterized by highest frequencies of *T. quinqueloba* (33.08%) and *G. bulloides* (26.04%). *Globigerinoides* spp. increase with values of 9%.

In general, the herbivorous group is always more abundant than carnivorous taxa showing a similar trend in both cores (Fig. ESM4). However, some fluctuations can be highlighted: five peaks of carnivorous taxa along CT10 core and two along LGT5 core. Though significant fluctuations, cold taxa are generally more abundant than warm ones, in both the cores (Figs. 6).

4.5. Age constraints and model

Age information derive from four radiocarbon ages and two cryptotephra ages. The radiometric ages and related calibrated ages (BP) obtained from radiocarbon analyses are listed in Table 2. The results indicate a calibrated age of 5991–5905 cal. yr BP and 3994–3854 cal. yr BP for the basal part of core CT10 and LGT5, respectively (Fig. 6). Sample CT10 164 has the youngest calibrated age (1298–1228 cal. yr BP). Sample LGT5 248 has a calibrated age of 1336–1446 cal. yr BP. Radiocarbon analysis indicates that the max. Age of the cored sections is ca. 6 ka. The two cryptotephra ages were obtained by samples CT1 and CT2, identified in core LGT5. Cryptotephra CT1 (299–300 cm bsf) consists of light grey high vesicular micropumices, sub-rounded to sub-angular in shape (Fig. ESM5) with phonolite composition, according to the Total Alkali-Silica classification diagram (TAS, Le Maitre, 2002; Fig. ESM6). Cryptotephra CT2 (169–170 cm bsf) is composed of transparent, aphyric and high vesicular micropumices with stretched bubbles (Fig. ESM5), and rhyolite composition, according to the TAS classification (Fig. ESM6). Further details of chemical composition of CT1 and CT2 cryptotephras are provided in Fig. ESM6. Available radiocarbon chronology for core LGT5 (Table 2), indicates that the two cryptotephra have an age younger than 4 ka. When compared with Late Holocene products from the main active volcanoes (Campi Flegrei, Somma-Vesuvius, Ischia Island, Aeolian Islands and Etna; e.g., Santacroce et al., 2008; Crocitti et al., 2019), the petrographic and chemical features of the CT1 micropumices result to be associated with the Vesuvius products, in particular with the products of the 79 CE eruption of Pompeii (see Fig. ESM6 for further details). The composition of crypto-tephra CT2 is typical of the high-K calc-alkaline series erupted by Aeolian arc volcanoes and in particular Lipari island (e.g., Peccerillo, 2017). Its stratigraphic position above cryptotephra CT1 correlated to Pompeii eruption, along with the comparison with available geochemical data (Caron et al., 2012; Crocitti et al., 2019; Fig. ESM6) suggest that cryptotephra CT2 can be correlated with the M. Pilato-Rocche Rosse eruption from Lipari Island (see Fig. ESM6 for further details) aged at 760 CE (1190 yr BP) and 1220 CE ± 30 (730 yr BP; Tanguy et al., 2003).

The various age information support the construction of the age model for core LGT5 and correlation between D50 and foraminifera warm-cold groups data on a age basis (Fig. 9); the age model for core LGT5 was obtained by linear interpolation between age constraint obtained from one ^{14}C date and cryptotephras CT1 and CT2. Differently, age information for core CT10 is insufficient to construct the age model, although radiocarbon ages and foraminiferal assemblages would indicate a Late Holocene age. Accumulation rates of ca. 1.1 mm/yr (sequence S2, between CT1 and 1386 yr BP radiocarbon age) and 1.9 mm/yr (sequences S2 and S3, between CT1 and CT2 cryptotephras) can be estimated for contourite deposits. Although some limitation might arise due to the low number of age control points and possible uncertainties derived by the use of organic matter for radiocarbon age determinations (Ausin et al., 2019), the coherency of age information obtained by tephras and radiocarbon age would suggest a rather consistent chronostratigraphic reconstruction. The model is also consistent with age information derived from foraminifera (Fig. ESM4): 1) the bottom of core LGT5 should belong to the basal part of ecobiozone 2F that started around 3700 BP; 2) close to the base of unit 3 a peak of carnivorous taxa at 140 cm in LGT5 might represent the end of the Dark Ages Cold Period (DACP; Lamb, 1995); 3) within unit 3, the warmer phase of the Medieval Warm Period at about 750 BP is possibly marked by a peak of *G. ruber* at 111 cm in LGT5. Moreover, a good correlation between the trend of warm-cold foraminifer groups with SST data from the Tyrrhenian Sea (Cacho et al., 2001) and Gulf of Lions (Jalali et al., 2016) is observed (Fig. 9).

4.6. Stratigraphic correlation

The correlation between seismic and core stratigraphy indicates that both the cores LGT5 and CT10 recovered sediments from seismic subunit SU2-E, SU2-D2 and SU2-D1 (Fig. 5). The homogeneous silty sediment of Unit 3, recovered in the upper part of both cores LGT5 and CT10 (Fig. 6), correlates with seismic subunit SU2-E that is characterized by semi-transparent facies. The silty sand interval with scattered lithic clasts

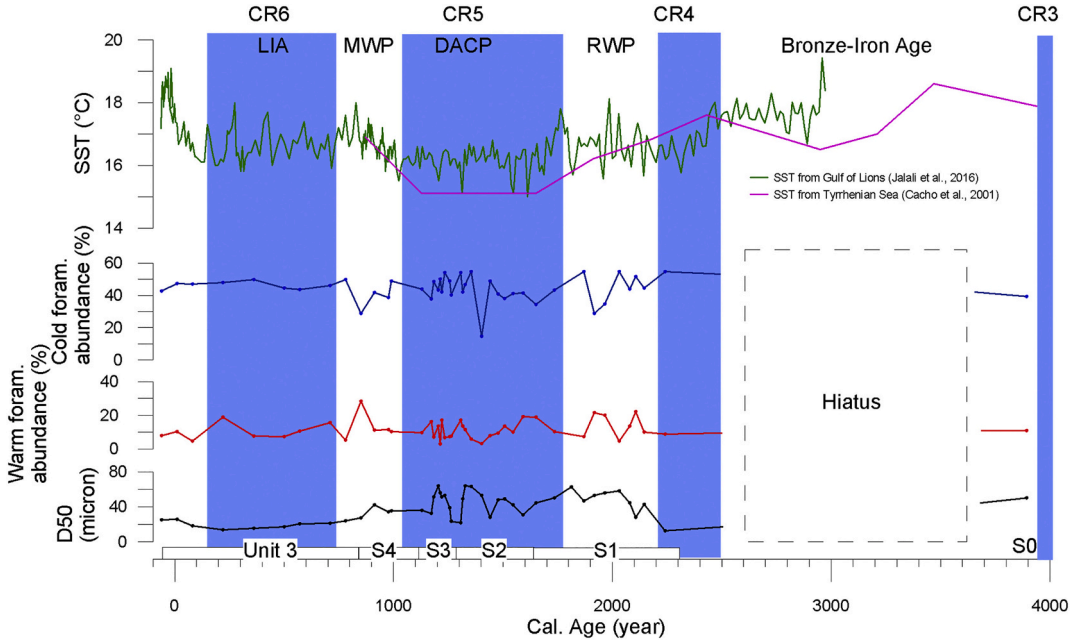

Fig. 9. Comparison of D50 and foraminifera warm-cold groups data for core LGT5 with indication of main climatic phases and SST data from the Mediterranean Sea (Cacho et al., 2001; Jalali et al., 2016). LIA: Little Ice Age (ca. 100–700 BP); MWP: Medieval Warm Period (ca. 700–1100 BP); DACP: Dark Ages Cold Period (ca. 1600–1100 BP); RWP: Roman Warm Period (ca. 2450 BP- 1600 BP). Climate periods from Helama et al. (2017). CR3, CR4, CR5 and CR6 indicate short cooling events from Jalali et al. (2016).

(Unit 1) recovered in the lower part of core CT10 possibly correlates with the upper part of seismic subunit SU2-D1. Lithological sub-units 2a and 2b correlate with seismic subunit SU2-D2 (Fig. 5). Thus, it is likely that the high-amplitude reflectors of this seismic unit are determined by the coarser-grained intervals forming the contourite sequences. In addition, seismic stratigraphy indicates that the sub-units 2a and 2b are likely coeval, as they belong to the same seismic subunit.

5. Discussion

5.1. Interpretation of Capo Vaticano deposits as contourites

The bi-gradational sequences identified in the cores (sub-units 2a and 2b) from the crest and moat sectors of the CS1 mounded-elongated drift point to the occurrence of sediment deposited under the action of along-slope geostrophic bottom currents, as observed grain size variations (Figs. 6, 7 and Table ESM1) are consistent with those described in the standard contourite facies model (Brackenridge et al., 2018; Stow and Smillie, 2020). This model of facies shows a negative grading (from muddy through silt-mottled to sandy sediment) and then a positive grading (back through to muddy facies) and the components of a complete sequence are indicated by the C1–C5 notation. Based on grain size data, coarser-grained intervals (silty-sand and sandy-silt) identified in sub-unit 2a and 2b would represent C3 divisions; finer-grained intervals (sandy-silt) can be associated to C2-C4 divisions and the finest ones to C1-C5 divisions (Tab. ESM1). Core LGT5 shows three complete bi-gradational sequences within sub-unit 2a (S1, S2 and S3) and one less-developed sequence (S4). Similarly, the three bi-gradational sequences observed in core CT10 (SII, SIII and SIV; sub-unit 2b) would reflect complete sequences of divisions C1-C5. The sequences are a few decimeters thick (24–65 cm) and based on visual observation there are no clear traces of large-scale and distinct burrows, however possible bioturbational mottling can be locally observed (Fig. ESM2a). The interpretation of bi-gradational sequences as contourite deposits is also sustained by correlation of lithological sub-units 2a and 2b with seismic subunit SU2-D2, characterized by sigmoidal to upward-convex external form, high amplitude facies and upslope migration (Rebesco and Stow, 2001). Further indication of deposition from bottom currents is provided by benthic foraminifera assemblages. Although these assemblages are very similar along the two cores and in the recent sediments (Di Bella et al., 2017), some differences can be identified between assemblages observed within the contourite sequences and muddy deposits forming Unit 3. Within the contourite sequences *G. subglobosa* is more abundant than *C. carinata*, which dominates the most recent assemblages (Unit 3), as also recorded in Cosentino et al. (2017). Although ecological factors determining the predominance of *G. subglobosa* over *C. carinata* and vice versa are still debated, in our case the greater abundance of *G. subglobosa* in the contourite sequences would highlight more oligotrophic conditions and enhanced bottom current velocities (Jorissen, 1987; Schmiedl et al., 1997; Martins et al., 2007; and references therein). Its capability to live in environments affected by intense bottom currents has been suggested in other settings, such as the Campos (de Mello e Sousa et al., 2006) and Gioia margins (Di Bella et al., 2017). *Cassidulina carinata* that is more abundant in muddy deposits of Unit 3 is the most important opportunistic species in recent eutrophic conditions in outer neritic and bathyal bottoms of the Mediterranean Sea (Blanc-Vernet, 1969; Sgarrella and Moncharmont-Zei, 1993; Abu Zied et al., 2008). This taxon is frequently recorded as epifaunal/shallow infaunal deposit feeders (Corliss and Fois, 1990; Murray, 2006; Zarries and Mackensen, 2010), indicative of intermediate organic carbon fluxes and high seasonality (Eberwein and Mackensen, 2008). In addition, the constant dominance of the planktonic herbivorous over the carnivorous group suggests the persistence of cold and nutrient-rich water masses during the whole time interval recorded by core sediments. These conditions would be consistent with the oceanographic characteristics of the study area and the presence of the modified-LIW in this depth interval.

As a whole, obtained results point to the occurrence of complete bi-gradational sequences arranged in a cyclic pattern, wherein a single sequence possibly formed during a multicentennial time interval. Since the bi-gradational grading generally develops over relatively longer time intervals (typically several millennia, Stow and Smillie, 2020), the Capo Vaticano sequences represent a high-resolution record of contourite sedimentation.

5.2. Other processes possibly interacting with contourite formation

Taking into account the geological and oceanographic setting of the study area further processes possibly interacting with formation of contourite sequences are outlined below.

5.2.1. Breaking of internal solitary waves

Breaking of internal solitary waves on sloping surfaces creates episodic and repetitive energetic events, able to induce an excess of bed shear stress that act on bottom sediment, thus generating resuspension and transport of bottom sediment (Cacchione and Wunsch, 1974; Reeder et al., 2011; Pomar et al., 2012; Yin et al., 2019; Miramontes et al., 2020). Typically, such a kind of high-turbulent events occur in mid-shelf settings, at the shelf edge, over the continental slope and in submarine canyons, depending on the depth at which interfaces between water masses intersect the sea floor (e.g., Ercilla et al., 2016).

South of Capo Vaticano (Fig. 1), Marullo and Santoleri (1986) hypothesized mixing processes at the interface between the LIW and the TSW, resulting from internal solitary wave breaking. According to these authors, and experimentally verified by La Forgia et al. (2018), internal solitary wave breaking events over the frontal slope of Capo Vaticano may cause high bottom shear stress and turbulent phenomena at the bottom layer. Sedimentological features observed in the study cores do not provide evidence of deposits that can be attributed to internal waves (e.g., cross lamination, rip-up clasts, cross bedding related to large-scale bedforms; Reeder et al., 2011; Bádenas et al., 2012; Gao et al., 2013). However, breaking of internal waves might provide an additional source of sediment that, in turn, can be entrained in the bottom current, and then redistributed along the geostrophic path. This hypothesis is supported by the spatial co-occurrence between −150 and − 250 m depth of: 1) sediment resuspension, forming a ca. 50 m thick nepheloid layer (sensu Dickson and McCave, 1986; Fig. 3); 2) the theoretical sector predicted by Cavaliere et al., 2020 for internal solitary wave breaking; and particularly 3) the shoreward thickening of the mixing-induced modified-LIW (see Section 4.1) that would testify the presence of internal solitary wave breaking phenomena. All this suggests a possible role of internal solitary waves in sediment resuspension with possible influence on contourite features.

5.2.2. Storm climate

As the study area is characterized by a very narrow shelf, a sedimentary linkage between the shelf and slope sector with off-shelf transport of sediment might be present (Harris and Wiberg, 2002; Bender et al., 2012) and variability of storm activity might exert a control in the accumulation of the contourite sequences. The shelf sediment export can be relevant in oceanic continental shelves, but less probable on the moderate-energy (lack of strong tides and swell waves) setting of the central Mediterranean shelves, where wave resuspension is mostly restricted to the inner shelf (e.g., Lo Iacono and Guillén, 2008). Therefore, a direct storm control on the formation of the Capo Vaticano sequences seems to be unlikely, unless stormier conditions occurred during their formation, as for instance suggested for the NW Mediterranean Sea during the Holocene (Sabatier et al., 2012).

5.2.3. Turbidity currents

In the study area turbidite systems, including submarine canyons and channels have been recognized by Martorelli et al. (2016). As the studied cores are located some kilometers northward from the Mesima canyon (i.e. downstream with respect to the flow of the modified-LIW, Fig. 2), the interaction between turbidite and contourite deposition might be possible. The distinction between down-slope and along-slope processes is not obvious and still controversial, even if recently it received attention (e.g., Mulder et al., 2008, 2013; Alonso et al., 2016; Ercilla et al., 2019). A consensus has been achieved on differences between these systems at a broad scale (depositional systems, architectural elements, seismic units), whereas diagnostic criteria at small-scale (cores and field) are still in debate and revision (e.g., Rebesco et al., 2014; Alonso et al., 2016; Stow and Smillie, 2020). In our case, the occurrence of complete bi-gradational sequences, along with the lack of normally-graded sequences that can be related to the classic turbidite facies models (Bouma, 1962; Stow, 1977; Lowe, 1982) and of sharp-erosional basal contacts, suggests the lack of significant interaction between these processes. The observation of similar dominant mode values within the sequences would also suggest the absence of turbidite deposition (interbedded turbidites would display different modes), in agreement with the distinguishing criteria proposed by Alonso et al. (2016). In addition, the lack of climbing ripples and the occurrence of symmetric to asymmetric sequences (with normally graded units that are usually thinner than the inversely graded units) also point to an opposite trend with respect to those type of turbidites generated by hyperpycnal flows (e.g., Mulder, 2011), possibly formed in the nearby area by the Mesima River.

5.3. Insights into sedimentary processes governing deposition of Capo Vaticano contourites and variability of deposition in the CS1 elongated drift

5.3.1. Comparison with textural features of other contourite deposits

The occurrence of well-developed and complete C1-C5 sequences provides the opportunity to gain information on sedimentary processes governing their deposition and to outline a small-scale variability in sedimentation. Capo Vaticano sequences have distinctive grain size signature that is similar to those recently described for sandy-silty and sandy contourites (Fig. 8; Brackenridge et al., 2018). A deeper look at grain size data indicates that vertical variations of grain size parameters (mean, sorting, kurtosis and skewness) in the contourite sequences follow specific trends within the units (Fig. 8 and Table ESM1), suggesting that they might provide additional information to distinguish different depositional processes (Brackenridge et al., 2018; Stow and Smillie, 2020). The main trends are:

i) Contourite sequences belonging to sub-unit 2a are generally characterized by an increase of sand percentage and sorting with increasing grain size, reaching maximum sand percentage and better sorting within C3 divisions (Fig. 8). Also Kurtosis has a distinctive trend of values (from platykurtic to leptokurtic) as grain size increases from C1-C5 divisions to C3 divisions. Moreover, sediment displays a progressively finer skewed distribution within the C3 divisions. The observed patterns are consistent with an overall gradual increase of current speed followed by a decrease, as commonly observed in stacked complete sequences (e.g., Stow and Faugeres, 2008). According to Brackenridge et al. (2018), the near symmetrical sediment distribution of fine-grained intervals (C1 and C5 divisions) is consistent with sediment deposited by settling from weak bottom currents, whereas the better sorting achieved in C3 divisions would indicate a decrease in deposition from the suspended load and increase of sediment deposited by the saltation load.

ii) In contourite sequences belonging to sub-unit 2b the trend of grain size features is less obvious and varies in the different sequences (Table ESM1, Fig. 8). In sequence SIV the trend are similar to those observed in sequences of sub-unit 2a. Sequences SII and SIII are characterized by a kurtosis trend with increasing grain size similar to the SIV trend but they show a decrease of sorting accompanied by a finer skewed distribution (sequence SIII) or by a near symmetrical distribution (sequence SII). These patterns differ from those observed in classic sequences and their interpretation is not straightforward. However, the observed decrease of sorting within C3 divisions might be determined by presence of coarse sediment (sand and microgravel).

iii) The portion of sequence recovered within Unit 1 is characterized by the coarsest sediment (D50 max. of 314 μm), poorest sorting and negative to positive skewness (tail of coarse-grained sediment). These distinctive grain size features would indicate deposition in a high-energy environment (e.g., an active moat channel), similar to sandy contourites

subject to winnowing (Stow et al., 2002c; Brackenridge et al., 2018).

iv) The muddy sediment composing the recent most deposit (Unit 3) represents hemipelagic sediment deposited under the influence of weak bottom currents, reflecting a general decrease of current speed.

5.3.2. *Variability of contourite sedimentation in the CS1 elongated drift and occurrence of sandy facies*

Changes in the textural characters of bi-gradational sequences indicate a variability of contourite sedimentation across drift CS1, both in space and in time. This variability is displayed also by seismic profiles, as both seismic sub-units SU2-D1 and SU2-D2 (i.e., the seismic subunits correlated with the cored contourite sequences) show different characteristics across the drift (moat and crest sectors). Although more information is needed to completely decipher these complex elements of the contourite system, hereafter we attempt to outline and discuss the main sedimentary features of moat and crest sectors and their variability through time (Fig. 10).

5.3.2.1. Drift crest sector. The drift crest sector, which is characterized by development of complete contourite sequences (S1, S2, S3) including sandy facies, likely reflects deposition of typical drift deposits (Drift deposit in Fig. 10b). These sequences developed in a rather similar way, without significant changes in sediment grain size features through the Late Holocene, probably as a consequence of the substantially fixed position of the crest sector through time (Fig. 5). In this sector, contourite deposits reach the maximum thickness (Fig. 10a, b), similarly to what is generally observed in elongated-separated drifts (e.g., Howe et al., 1994). Interestingly, the examined cores indicate that C1 and C5 divisions of contourite sequences also contribute to the thickening of the deposits in the crest sector. This should be consistent with observation of an increased thickness of muddy facies laterally away from the main current core (Brackenridge et al., 2018).

5.3.2.2. Moat sector. Both seismic and core data indicate a more complex sedimentation in the moat sector with development of different deposits through time. It includes thin complete contourite sequences (sub-unit 2b) with variable grain size features, coarse-grained deposits (Unit 1) evidence of erosion/non deposition and reworking (Fig. 10a). According to Martorelli et al. (2016), seismic profiles indicate that the moat migrated upslope through time (see deposition of subunit SU2-D2 and SU2-D1). "True" moat deposits are likely represented by deposits forming Unit 1 (D50 max. of 314 μm, with lithic clast up to 0.5 cm in size, with poorest sorting among the cored succession) that developed in a moat active during emplacement of seismic sub-unit SU2-D1 (ca. 6000 cal. yr BP; Fig. 10a), where high energy conditions determined also the slight reworking observed on seismic profiles. Differently, during the successive emplacement of seismic sub-unit SU2-D2 (Fig. 10), the moat sector is characterized by deposition of contourite sequences (SII, SIII and SIV), whose grain size features differ from those of standard contourite sequences (Fig. 8). Here, seismic profiles possibly indicate that this sector is influenced by sedimentation of the distal-finer portion of drift deposits (Fig. 10b), likely favored by the progressive upslope migration of the active moat, which hampered erosive-bypass processes allowing local accumulation of distal drift deposits. Actually, this interpretation is not obvious, as in separated drifts the moat is commonly described as a non-depositional/erosive area or is characterized by sedimentation under higher energy condition (Rebesco et al., 2014 and references therein), although it may host different type of deposits (e.g., turbidites and hemipelagites; Lebreiro et al., 2015).

To summarize, the above features indicate a more complex pattern of sedimentation in the moat sector than the crest, highlighting a dynamic environment where different deposits may develop through time, and suggesting that during the evolution of elongated-separated drifts this sector can host sedimentation related both to "true" moat processes and to distal-lateral deposition of sediment forming drift deposits. This finding would highlight that further studies are needed to completely decipher this complex environment.

It is also noteworthy that, Capo Vaticano deposits include coarser sandy facies that occur as moat-related lag deposits, and finer sandy facies that form C3 divisions of complete bi-gradational sequences accumulated on drift deposits close to the crest sector. This finding is relevant because generally sand-rich contourites are relatively rare along the continental margins and sandy sequences are generally truncated (or absent), if compared to finer-grained successions (Stow and Smillie, 2020). Analogously to other examples of sandy contourites recognized along the upper sector of the continental slope, such as the Faro drift in the Gulf of Cadiz (Gonthier et al., 1984; Stow et al., 2002b), the Brazilian margin-Campos slope (Viana et al., 2002) and the northern Tyrrhenian Sea (Miremontes et al., 2016), the occurrence of sandy facies offshore Capo Vaticano would highlight that relatively shallow water-energetic environments impacted by surface or intermediate water masses and proximal to sandy sources may represent favorable settings for accumulation of sandy sediment. In addition, the finding of sandy facies close to the crest sector of drift deposits would indicate that at shallow depths these sectors can represent favorable settings for accumulation of sandy contourites.

5.4. *Imprint of millennial- and multicentennial-scale bottom current variability in Capo Vaticano contourites*

Seismic stratigraphy indicates that drift CS1 formed during the post-LGM period. Both cores sampled the upper part of drift CS1 (subunits SU2-D2 and SU2-E, Fig. 5) where geochronological constraint, indicate that they approximately span the time interval of the middle-late Holocene (Fig. 10). The architecture of drift CS1, including several seismic subunits separated by non-depositional/erosive surfaces, and the finding of complete bi gradational sequences within the sediment cores, would indicate variations of contourite sedimentation at different timescales. Due to the shallow setting of the study area, cyclic variations of contourite sedimentation recorded by seismic units composing drift CS1 can be attributable to fluctuations of bottom current activity mostly governed by sea-level changes and climate variations. In fact, during the Late Quaternary high-amplitude glacio-eustatic sea level changes (with a ca, 120 m lowered sea-level during the LGM period; Peltier and Fairbanks, 2006) affected the distribution of water masses, depth of interfaces and overall architecture of drift CS1. The erosive character of the lower boundary (ES in Fig. 5) of drift CS1 might indicate that vigorous bottom currents occurred around the LGM period, although, these currents were likely related to a surface water mass as the sea-level was considerably lower. Differently, in the upper part of drift CS1 (e.g., seismic subunits SU2-D1, D2 and E, Figs. 4 and 5) the deposits formed during the Holocene highstand period, when the sea level approached its present position. Therefore, bottom currents responsible for their formation can be related to an intermediate water mass, likely represented by the paleo modified-LIW (Figs. 1 and 3). For Holocene deposits sea level variations can be considered subordinate, whereas climate factors operating at different time scales would have played a major role. It is well known that climate variability and intermediate/deep-water circulation are intimately linked (e.g., Rohling et al., 2015), with rapid cooling (e.g., D/O stadials) and warming events (e.g., D/O interstadials) superimposed on the Milankovitch forcing. In the Mediterranean, these climatic events promoted enhancement or reduction of the circulation during colder and warmer periods, respectively (e.g., Cacho et al., 2000; Frigola et al., 2008; Angue Minto'o et al., 2015; Tripsanas et al., 2016). In the northern Tyrrhenian Sea, recent studies (Toucanne et al., 2012; Angue Minto'o et al., 2015; Miramontes et al., 2016) recognized high-frequency (millennial-scale) variations of contourite sedimentation related to the variability of LIW, with a weaker activity during late Quaternary warm periods and faster currents during major cold periods (e.g. the last glacial interval and the Younger Dryas). In this scenario, we surmise that variations of contourite sedimentation recorded by seismic

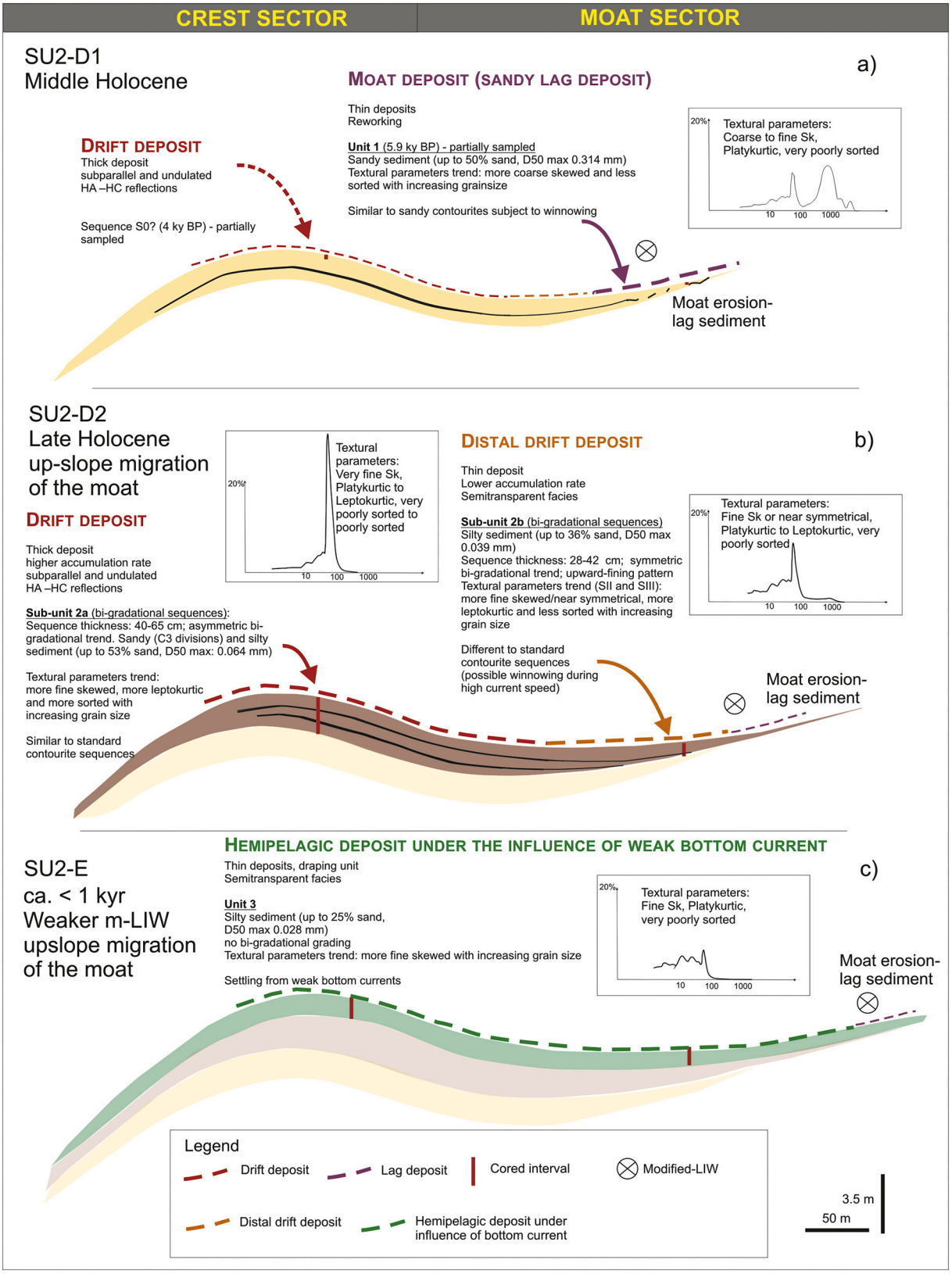

Fig. 10. Scheme showing evolution of drift CS1 during the Middle-Late Holocene with synthesis of seismostratigraphic and lithologic features of Capo Vaticano contourite sequences and indication of different types of contourite deposits.

units composing drift CS1 might reflect modified-LIW variability driven by climate fluctuations on a millennial-scale. Moreover, the stacked C1-C5 contourite sequences forming lithological sub-units 2a and 2b would indicate cyclical variations in the activity of bottom current (Stow and Faugeres, 2008), which can be related to shorter climate variations (possibly multicentennial-scale) of the middle-late Holocene period. In fact, as these sequences developed during a period characterized by a stable sea level, rapid climate events may explain their development. This finding would be consistent with the Holocene short-term climatic variability, including relevant rapid cooling events occurring at millennial-centennial scale (e.g., Mayewski et al., 2004). In particular, in the western Mediterranean region several short cooling events have been recognized, although the timing, extent and intensity can be variable (e.g., Cacho et al., 2001; Jalali et al., 2016). Recent high-resolution studies (e.g., Schilman et al., 2001) demonstrated that during the late Holocene period a complex climatic instability occurred also in the eastern Mediterranean, with implications on formation and circulation of the LIW and other water masses (Tripsanas et al., 2016). The comparison between the age of contourite sequences with major climate events of the late Holocene and SST records from the Tyrrhenian Sea (Cacho et al., 2001) and Gulf of Lions (Fig. 9; Jalali et al., 2016) suggests that sequences S2 and S3 developed during a major cooling event (i.e., the CR5 event reported by Jalali et al., 2016, corresponding to the TC1 and AC1 cooling events reported by Cacho et al., 2001). This event can be traced in both the western and eastern Mediterranean Sea and corresponds to the Dark Age Cold Period (DACP, ca. 1600–1100 yr BP; Jalali et al., 2016; Helama et al., 2017). Moreover, we observe a good correspondence between the greater abundance of cold planktonic foraminifera taxa and coarser intervals of contourite sequences (Fig. 9). A similar relation has been observed in the Corsica trough (Tyrrhenian Sea) during major post-LGM cold episodes (e.g., the Younger Dryas; Angue Minto'o et al., 2015) and in the Aegean Sea for cascading bottom currents (Tripsanas et al., 2016). As a whole, these findings seem to highlight that periods of enhanced bottom currents likely occurred during colder phases of the Late Holocene, while weaker regimes might be related to warmer phases. In this regard, further research will provide a better understanding between variations of bottom currents and climate variability, for example determining the influence of other climatic factors and extending the stratigraphic record and chronological constraint.

6. Conclusions

The integrated study of high-resolution seismic profiles and sediment characteristics of contourite deposits derived from two short sediment cores collected from a contourite drift on the upper continental slope of the Capo Vaticano margin (Tyrrhenian Sea) revealed significant information on contourite deposition during the mid-to-late Holocene period. A new refined seismic analysis reveals that depositional architecture of contourites is characterized by several sub-units, an upslope migration of the moat sector and a relatively stable position of the crest sector. The sediment core data allowed us to detail for the first time the characteristics of these contourite deposits, including complete bi-gradational contourite sequences. The main conclusions are:

1. Capo Vaticano contourite deposits are composed of stacked bi-gradational C1-C5 sequences formed by a bottom current related to an intermediate water mass, likely similar to the present-day modified-LIW issued from the Messina Strait. A significant interaction between along-slope and down-slope processes can be excluded in this sector, at the scale of sediment cores.
2. Capo Vaticano contourites include sandy deposits, accumulated as lag deposits formed in active moats or as C3 intervals of contourite bi-gradational sequences. The finding of sandy contourites is significant as these deposits are still poorly known and would highlight their promising occurrence in continental slope settings impacted by intermediate/surface waters.
3. The observed variability in contourite deposits mostly reflects differences in sedimentary processes occurring within a contourite drift system, specifically in the crest and distal portion/moat sectors of the drift. Accumulation rates and grain size vary across crest and moat sectors of drift deposit. In particular, the moat sector seems to be characterized by a more complex stratigraphic record where different depositional processes may develop through time.
4. Capo Vaticano contourites provide evidence of rapid (e.g., multicentennial) changes of modified-LIW activity in the southern Tyrrhenian Sea during the middle-late Holocene. We surmise that these changes are controlled by climate fluctuations. According to the proposed stratigraphic reconstruction, periods of enhanced bottom current speeds likely developed during colder events, whereas activity of bottom-currents decreased during the last part of the late Holocene period and warmer oscillations.

It is worth to notice that Capo Vaticano contourites represent a relatively rare example of complete C1-C5 bi-gradational sequences, which include sandy facies, and are arranged in a high-frequency cyclic stacking pattern. These deposits provide a very high-resolution archive of contourite processes and cyclicity, possibly reflecting climate variations that deserve to be more thoroughly studied. Moreover, the hypothesis of a specific role of internal solitary waves in sediment resuspension and seabed reshaping over this region sets future observational and numerical investigations, aimed at exploring their potential influence on contourite features.

Supplementary data to this article can be found online at https://doi.org/10.1016/j.margeo.2020.106372.

Declaration of Competing Interest

The authors declare that they have no known competing financial interests or personal relationships that could have appeared to influence the work reported in this paper.

Data availability

The datasets analysed during the current study are available from the corresponding author on reasonable request.

Acknowledgements

The data used in this study were collected by CNR-IGAG (Rome, Italy) aboard of the Urania and Minerva1 research vessels. We would like to thank captains, crews and participants of the oceanographic cruises. G. Macelloni, M. Serracino and M. Albano are gratefully acknowledged for their contribution in grain size, EDS and SEM analyses, respectively. We thank the Editor M. Rebesco, D. Van Rooij, E. Miramontes, E. Tripsanas and two anonymous reviewers for their fruitful comments and suggestions that greatly improved the manuscript. Core LGT5 was collected during the Gioia77 cruise funded by the Eurofleets2 Project.

References

Abu Zied, R.H., Rohling, E.J., Jorissen, F.J., Fontanier, C., Casford, J.S.L., Cooke, S., 2008. Benthic foraminiferal response to changes in bottom water oxygenation and organic carbon flux in the eastern Mediterranean during LGM to recent times. Mar. Micropaleontol. 67, 46–68.

Alonso, B., Ercilla, G., Casas, D., Stow, D.A., Rodríguez-Tovar, F.J., Dorador, J., Hernández-Molina, F.J., 2016. Contourite vs gravity-flow deposits of the Pleistocene Faro Drift (Gulf of Cadiz): sedimentological and mineralogical approaches. Mar. Geol. 377, 77–94.

Alpers, W., Salusti, E., 1983. Scylla and Charybdis observed from space. J. Geophys. Res. Oceans 88 (C3), 1800–1808.

Angue Minto'o, C.A., Bassetti, M.A., Morigi, C., Ducassou, E., Toucanne, S., Jouet, G., Mulder, T., 2015. Levantine intermediate water hydrodynamic and bottom water ventilation in the northern Tyrrhenian Sea over the past 56,000 years: New insights from benthic foraminifera and ostracods. Quat. Int. 357, 295–313.

Antonioli, F., Ferranti, L., Lambeck, K., Kershaw, S., Verrubbi, V., Dai Pra, G., 2006. Late Pleistocene to Holocene record of changing uplift rates in southern Calabria and northeastern Sicily (southern Italy, Central Mediterranean Sea). Tectonophysics 422 (1–4), 23–40.

Bádenas, B., Pomar, L., Aurell, M., Morsilli, M., 2012. A facies model for internalites (internal wave deposits) on a gently sloping carbonate ramp (Upper Jurassic, Ricla, NE Spain). Sediment. Geol. 271, 44–57.

Bahr, A., Jiménez-Espejo, F.J., Kolasinac, N., Grunert, P., Hernández-Molina, F.J., Röhl, U., Alvarez-Zarikian, C.A., 2014. Deciphering bottom current velocity and paleoclimate signals from contourite deposits in the Gulf of Cádiz during the last 140 kyr: An inorganic geochemical approach. Geochemistry, Geophysics, Geosystems 15 (8), 3145–3160.

Bender, V.B., Hanebuth, T.J., Mena, A., Baumann, K.H., Francés, G., von Dobeneck, T., 2012. Control of sediment supply, palaeoceanography and morphology on late Quaternary sediment dynamics at the Galician continental slope. Geo-Mar. Lett. 32 (4), 313–335.

Blanc-Vernet, L., 1969. Contribution a l'etude des foraminiferes de Mediterranee. Theses de Doctorat Etat. Travaux de la Station Marine d'Endoume, Marseille, 281 pp.

Blott, S.J., Pye, K., 2001. GRADISTAT: a grain size distribution and statistics package for the analysis of unconsolidated sediments. Earth Surf. Process. Landf. 26 (11), 1237–1248.

Bosman, A., Casalbore, D., Dominici, R., 2017. Cyclic steps at the head of channelized features along the Calabrian margin (Southern Tyrrhenian Sea, Italy). In: Guillén, J., Acosta, J., Chiocci, F., Palanques, A. (Eds.), Atlas of Bedforms in the Western Mediterranean. Springer, Cham.

Bouma, A.H., 1962. Sedimentology of some Flysch deposits; a graphic approach to facies interpretation, 1043. Elsevier Pub.

Brackenridge, R.E., Stow, D.A., Hernández-Molina, F.J., Jones, C., Mena, A., Alejo, I., Perez-Arlucea, M., 2018. Textural characteristics and facies of sand-rich contourite depositional systems. Sedimentology 65 (7), 2223–2252.

Brandt, P., Rubino, A., Quadfasel, D., Alpers, W., Sellschopp, J., Fiekas, H.-V., 1999. Evidence for the influence of Atlantic–Ionian stream fluctuations on the tidally induced internal dynamics in the Strait of Messina. J. Phys. Oceanogr. 29 (5), 1071–1080.

Cacchione, D., Wunsch, C., 1974. Experimental study of internal waves over a slope. J. Fluid Mech. 66 (2), 223–239.

Cacho, I., Grimalt, J.O., Sierro, F.J., Shackleton, N., Canals, M., 2000. Evidence for enhanced Mediterranean thermohaline circulation during rapid climatic coolings. Earth Planet. Sci. Lett. 183 (3–4), 417–429.

Cacho, I., Grimalt, J.O., Canals, M., Sbaffi, L., Shackleton, N.J., Schönfeld, J., Zahn, R., 2001. Variability of the western Mediterranean Sea surface temperature during the last 25,000 years and its connection with the Northern Hemisphere climatic changes. Paleoceanography 16 (1), 40–52.

Caron, B., Siani, G., Sulpizio, R., Zanchetta, G., Paterne, M., Zanella, E., 2012. Late Pleistocene to Holocene tephrostratigraphic record from the Northern Ionian Sea. Mar. Geol. 311, 41–51.

Casalbore, D., Falcini, F., Martorelli, E., Morelli, E., Bosman, A., Calarco, M., Chiocci, F. L., 2018. Characterization of overbanking features on the lower reach of the Gioia-Mesima canyon-channel system (southern Tyrrhenian Sea) through integration of morpho-stratigraphic data and physical modeling. Prog. Oceanogr. 169, 66–78.

Cavaliere, D., La Forgia, G., Adduce, C., Alpers, W., Martorelli, E., Falcini, F., 2020. Breaking location of Internal Solitary Waves: analytical model and experimental validation over a sloping seabed. Journal of Geophysical Research-Oceans. https://doi.org/10.1029/2020JC016669 (Accepted).

Cimerman, F., Langer, M., 1991. Mediterranean foraminifera. In: Slovenska Akademija Znanosti Umetnosti, Academia Scientiarum Artium Slovenica, Classis IV: Historia Naturalis, 30, pp. 1–118.

Cita, M.B., Vergnaud-Grazzini, C., Robert, C., Chamley, H., Ciaranfi, N., d'Onofrio, S., 1977. Paleoclimatic record of a long deep sea core from the Eastern Mediterranean. Quat. Res. 8, 205–235.

Colantoni, P., Gennesseaux, M., Vanney, J.R., et al., 1992. Processi dinamici del canyon sottomarino di Gioia Tauro (Mare Tirreno). Giorn. Geol. 3 (54/2), 199–213.

Corliss, B.H., Fois, E., 1990. Morphotype analysis of deep-sea benthic foraminifera from the northwest Gulf of Mexico. Palaios 5, 589–605.

Cosentino, C., Molisso, F., Scopelliti, G., Caruso, A., Insinga, D.D., Lubritto, C., Pepe, F., Sacchi, M., 2017. Benthic foraminifera as indicators of relative sea-level fluctuations: Paleoenvironmental and paleoclimatic reconstruction of a Holocene marine succession (Calabria, south-eastern Tyrrhenian Sea). Quat. Int. 439, 79–101.

Crocitti, M., Sulpizio, R., Insinga, D.D., De Rosa, R., Donato, P., Iorio, M., Zanchetta, G., Barca, D., Lubritto, C., 2019. On ash dispersal from moderately explosive volcanic eruptions: Examples from Holocene and Late Pleistocene eruptions of Italian volcanoes. Journal of Volcanology and Geothermal Research 385, 198–221.

CPTI Working Group, 2004. Catalogo Parametrico dei Terremoti Italiani, versione 2004 (CPTI04). INGV, Bologna. http://emidius.mi.ingv.it/CPTI.

De Mello e Sousa, S.H., M., D., Passos, R.F., Fukumoto, M., da Silveira, I.C.A., Figueira, R. C.L., Koutsoukos, E.A., Rezende, C.E., 2006. Mid-lower bathyal benthic foraminifera of the Campos Basin, Southeastern Brazilian margin: biotopes and controlling ecological factors. Marine Micropaleontology 61 (1-3), 40–57.

Di Bella, L., Pierdomenico, M., Porretta, R., Chiocci, F.L., Martorelli, E., 2017. Living and dead foraminiferal assemblages from an active submarine canyon and surrounding sectors: the Gioia Canyon system (Tyrrhenian Sea, Southern Italy). Deep-Sea Res. I 123, 129–146.

Dickson, R.R., McCave, I.N., 1986. Nepheloid layers on the continental slope west of Porcupine Bank. Deep Sea Res. Part A Oceanogr. Res. Pap. 33 (6), 791–818.

Droghei, R., Falcini, F., Casalbore, D., Martorelli, E., Mosetti, R., Sannino, G., Santoleri, R., Chiocci, F.L., 2016. The role of Internal Solitary Waves on deep-water sedimentary processes: the case of up-slope migrating sediment waves off the Messina Strait. Sci. Rep. 6, 36376.

Eberwein, A., Mackensen, A., 2008. Last Glacial Maximum paleoproductivity and water masses off NW-Africa: Evidence from benthic foraminifera and stable isotopes. Marine Micropal 67 (1-2), 87–103.

Ercilla, G., Juan, C., Hernández-Molina, F.J., Bruno, M., Estrada, F., Alonso, B., Vazquez, J.T., 2016. Significance of bottom currents in deep-sea morphodynamics: an example from the Alboran Sea. Marine Geology 378, 157–170.

Ercilla, G., Juan, C., Periáñez, R., Alonso, B., Abril, J.M., Estrada, F., El Moumni, B., 2019. Influence of alongslope processes on modern turbidite systems and canyons in the Alboran Sea (southwestern Mediterranean). Deep Sea Research Part I: Oceanographic Research Papers 144, 1–16.

Fabbri, A., Ghisetti, F., Vezzani, L., 1980. The Peloritani-Calabria range and the Gioia basin in the Calabrian arc (Southern Italy): relationships between land and marine data. Geol. Romana 19, 131–150.

Folk, R., Ward, W., 1957. Brazos River Bar: a study in the significance of grain size parameters. J. Sediment. Petrol. 27, 3–26.

Frigola, J., Moreno, A., Cacho, I., Canals, M., Sierro, F.J., Flores, J.A., Grimalt, J.O., 2008. Evidence of abrupt changes in Western Mediterranean Deep Water circulation during the last 50 kyr: a high-resolution marine record from the Balearic Sea. Quat. Int. 181 (1), 88–104.

Galli, P., Scionti, V., & Spina, V. 2004. New paleoseismic data from the Lakes and Serre faults (Calabria). Proc. of the 23 rd GNGTS.

Gao, Z., He, Y., Li, X.D., Duan, T., Wang, Y., Liu, M., 2013. Review of research in internal-wave and internal-tide deposits of China. J. Palaeogeogr. 2 (1), 56–65.

Gonthier, E., Faugeres, J.-C., Stow, D., 1984. Contourite facies of the Faro Drift, Gulf of Cadiz. In: Stow, D., Piper, D. (Eds.), Fine-Grained Sediments: Deep-Water Processes and Facies. Geological Society Special Publication, London, pp. 275–292.

Hanebuth, T.J., Zhang, W., Hofmann, A.L., Löwemark, L.A., Schwenk, T., 2015. Oceanic density fronts steering bottom-current induced sedimentation deduced from a 50 ka contourite-drift record and numerical modeling (off NW Spain). Quat. Sci. Rev. 112, 207–225.

Harris, C.K., Wiberg, P., 2002. Across-shelf sediment transport: interactions between suspended sediment and bed sediment. J. Geophys. Res. Oceans 107 (C1), 1–8.

Helama, S., Jones, P.D., Briffa, K.R., 2017. Dark Ages Cold Period: a literature review and directions for future research. The Holocene 27, 1600–1606.

Hemleben, C., Spindler, M., Anderson, O.R., 1989. Modern Planktonic Foraminifera. Springer-Verlag, New York, p. 363.

Hernández-Molina, F.J., Wåhlin, A., Bruno, M., Ercilla, G., Llave, E., Serra, N., Roque, D., 2016. Oceanographic processes and morphosedimentary products along the Iberian margins: A new multidisciplinary approach. Marine Geology 378, 127–156.

Hopkins, T.S., 1988. Recent Observations on the Intermediate and Deep Water Circulation in the Southern Tyrrhenian Sea Oceanol. Acta Spec. Issue.

Hopkins, T.S., Salusti, E., Settimi, D., 1984. Tidal forcing of the water mass interface in the strait of Messina J. Geophys. Res. 89 (C2), 2013–2024.

Howe, J.A., Stoker, M.S., Stow, D.A.V., 1994. Late Cenozoic sediment drift complex, northeast Rockall Trough, North Atlantic. Paleoceanography 9 (6), 989–999.

Iaccarino, S.M., Premoli Silva, I., Biolzi, M., Foresi, L.M., Lirer, F., Turco, E., Petrizzo, M. R., 2007. Practical Manual of Neogene Planktonic Foraminifera. International School on Planktonic Foraminifera, 6th course, Perugia 19–23 February 2007. University of Perugia, pp. 1–181.

Jalali, B., Sicre, M.A., Bassetti, M.A., Kallel, N., 2016. Holocene climate variability in the north-western Mediterranean Sea (Gulf of Lions). Clim. Past Discuss. 12, 91–120.

Jones, P.D., Mann, M.E., 2004. Climate over past millennia. Rev. Geophys. 42, RG2002.

Jorissen, F.J., 1987. The distribution of benthic foraminifera in the Adriatic Sea. Mar. Micropaleontol. 12, 21–48.

Kennet, J.P., Snivrasan, M.S., 1983. Neogene Planktonic Foraminifera. A Phylogenetics Atlas. Hutchinson Ross Publishing Company, New York.

Knutz, P.C., 2008. Paleoceanographic significance of contourite drifts. In: Contourites, M. Rebesco, Camerlenghi, A. (Eds.), Developments in Sedimentology, 60. Elsevier, pp. 511–535.

La Forgia, G., Adduce, C., Falcini, F., 2018. Laboratory investigation on internal solitary waves interacting with a uniform slope. Adv. Water Resour. 120, 4–18.

Lamb, H.H., 1995. Climate History and the Modern World, 2nd edition. Routledge, New York.

Lascaratos, A., Roether, W., Nittis, K., Klein, B., 1999. Recent changes in deep water formation and spreading in the eastern Mediterranean Sea: a review. Prog. Oceanogr. 44 (1–3), 5–36.

Lebreiro, SM., Antón L., Reguera M.I., Fernández M., Conde E., Barrado A.I., Yllera A., 2015. Zooming into the Mediterranean outflow fossil moat during the 1.2–1.8

million years period (Early-Pleistocene)—an approach by radiogenic and stable isotopes. Glob. Planet. Chang. 135, 104–118.
Lebreiro, S.M., Antón, L., Reguera, M.I., Marzocchi, A., 2018. Paleoceanographic and climatic implications of a new Mediterranean Outflow branch in the southern Gulf of Cadiz. Quat. Sci. Rev. 197, 92–111.
Lirer, F., Sprovieri, M., Ferraro, L., Vallefuoco, M., Capotondi, L., Cascella, A., Petrosino, P., Insinga, D.D., Pelosi, N., Tamburrino, S., Lubritto, C., 2013. Integrated stratigraphy for the late Quaternary in the eastern Tyrrhenian Sea. Quat. Int. 292, 71–85.
Llave, E., Schönfeld, J., Hernández-Molina, F.J., Mulder, T., Somoza, L., Del Río, V.D., Sánchez-Almazo, I., 2006. High-resolution stratigraphy of the Mediterranean outflow contourite system in the Gulf of Cadiz during the late Pleistocene: the impact of Heinrich events. Mar. Geol. 227 (3–4), 241–262.
Lo Iacono, C., Guillén, J., 2008. Environmental conditions for gravelly and pebbly dunes and sorted bedforms on a moderate-energy inner shelf (Marettimo Island, Italy, western Mediterranean). Cont. Shelf Res. 28 (2), 245–256.
Loeblich, A.R., Tappan, H., 1987. Foraminiferal Genera and their Classification. Van Nostrand Reinhold Comp., New York 970 p.44.
Lowe, D.R., 1982. Sediment gravity flows; II, Depositional models with special reference to the deposits of high-density turbidity currents. J. Sediment. Petrol. 52, 279–297.
Maitre, Le, et al., 2002. In: W. (Ed.), A Classification of Igneous Rocks and Glossary of Terms, 2nd edition. Cambridge University Press. 236 pp.
Margaritelli, G., Vallefuoco, M., Di Rita, F., Capotondi, L., Bellucci, L.G., Insinga, D.D., Petrosino, P., Bonomo, S., Cacho, I., Cascella, A., Ferraro, R., Lirer, F., 2016. Marine response to climate changes during the last five millennia in the central Mediterranean Sea. Global and Planetary change 142, 53–72.
Martins, V., Dubert, J., Jouanneau, J.-M., Weber, O., Ferreira da Silva, E., Patinha, C., Alveirinho Dias, J.M., Rocha, F., 2007. A multiproxy approach of the Holocene evolution of shelf-slope circulation on the NW Iberian Continental Shelf. Mar. Geol. 239, 1–18.
Martorelli, E., Bosman, A., Casalbore, D., Falcini, F., 2016. Interaction of down-slope and along-slope processes off Capo Vaticano (southern Tyrrhenian Sea, Italy), with particular reference to contourite-related landslides. Mar. Geol. 378, 43–55.
Marullo, S., Santoleri, R., 1986. Fronts and internal currents at the northern mouth of the Strait of Messina. Nuovo Cimento 9 (3), 701–713.
Mayewski, P.A., Rohling, E., Stager, C., et al., 2004. Holocene climate variability. Quat. Res. 62, 243–255.
Miramontes, E., Cattaneo, A., Jouet, G., Théreau, E., Thomas, Y., Rovere, M., Trincardi, F., 2016. The Pianosa contourite depositional system (northern Tyrrhenian Sea): drift morphology and plio-quaternary stratigraphic evolution. Marine Geology 378, 20–42.
Miramontes, E., Jouet, G., Thereau, E., Bruno, M., Penven, P., Guerin, C., Thiéblemont, A., 2020. The impact of internal waves on upper continental slopes: insights from the Mozambican margin (southwest Indian Ocean). Earth Surface Processes and Landforms 45 (6), 1469–1482.
Mosher, D.C., Campbell, D.C., Gardner, J.V., Piper, D.J.W., Chaytor, J.D., Rebesco, M., 2017. The role of deep-water sedimentary processes in shaping a continental margin: the Northwest Atlantic. Mar. Geol. 393, 245–259.
Mulder, T., 2011. Gravity processes and deposits on continental slope, rise and abyssal plains. In: Developments in Sedimentology, 63. Elsevier, pp. 25–148.
Mulder, T., Faugéres, J.C., Gonthier, E., 2008. Mixed turbidite-contourite systems. In: Contourites, M. Rebesco, Camerlenghi, A. (Eds.), Developments in Sedimentology, 60. Elsevier, pp. 435–456.
Mulder, T., Hassan, R., Ducassou, E., Zaragosi, S., Gonthier, E., Hanquiez, V., Toucanne, S., 2013. Contourites in the Gulf of Cadiz: a cautionary note on potentially ambiguous indicators of bottom current velocity. Geo-Marine Letters 33 (5), 357–367.
Murray, J.W., 2006. Ecology and Applications of Benthic Foraminifera. Cambridge University Press, Cambridge.
Peltier, W.R., Fairbanks, R.G., 2006. Global glacial ice volume and Last Glacial Maximum duration from an extended Barbados sea level record. Quat. Sci. Rev. 25 (23–24), 3322–3337.
Pierdomenico, M., Martorelli, E., Dominguez-Carrió, C., Gili, J.M., Chiocci, F.L., 2016. Seafloor characterization and benthic megafaunal distribution of an active submarine canyon and surrounding sectors: the case of Gioia Canyon (Southern Tyrrhenian Sea). J. Mar. Syst. 157, 101–117.
Pomar, L., Morsilli, M., Hallock, P., Bádenas, B., 2012. Internal waves, an under-explored source of turbulence events in the sedimentary record. Earth Sci. Rev. 111 (1–2), 56–81.
Pouchou, J.L., Pichoir, F., 1991. Quantitative analysis of homogeneous or stratified microvolumes applying the model "PAP". In: Electron Probe Quantitation. Springer, Boston, MA, pp. 31–75.
Povero, P., Hopkins, T.S., Fabiano, M., 1990. Oxygen and nutrient observations in the southern Tyrrhenian Sea. Oceanol. Acta 13 (3), 299–305.
Pujol, C., Vergnaud-Grazzini, C., 1995. Distributions patterns of living planktonic foraminifers as related to regional hydrography and productive systems of the Mediterranean Sea. Mar. Micropaleontol. 25, 187–217.
Ramsey, C.B., 2009. Bayesian analysis of radiocarbon dates. Radiocarbon 51 (1), 337–360.
Rebesco, M., Stow, D.A.V., 2001. Seismic expression of contourites and related deposits: a preface. Mar. Geophy. Researches 22, 303–308.
Rebesco, M., Hernández-Molina, F.J., Van Rooij, D., Wåhlin, A., 2014. Contourites and associated sediments controlled by deep-water circulation processes: state-of-the-art and future considerations. Mar. Geol. 352, 111–154.
Reeder, D.B., Ma, B.B., Yang, Y.J., 2011. Very large subaqueous sand dunes on the upper continental slope in the South China Sea generated by episodic, shoaling deep-water internal solitary waves. Mar. Geol. 279 (1–4), 12–18.
Reimer, P.J., Bard, E., Bayliss, A., Beck, J.W., Blackwell, P.G., Grootes, P.M., 2013. IntCal13 and Marine13 radiocarbon age calibration curves 0–50,000 years cal BP. Radiocarbon 55 (4), 1869–1887.
Robinson, A.R., Leslie, W.G., Theocharis, A., Lascaratos, A., 2001. Mediterranean Sea circulation. Ocean Curr. 1, 19.
Rohling, E.J., Jorissen, F.J., Vergnaud-Grazzini, C., Zachariasse, W.J., 1993. Northern Levantine and Adriatic Quaternary planktic foraminifera; Reconstruction of paleoenvironmental gradients. Mar. Microplaleontol. 21, 191–218.
Rohling, E.J., Marino, G., Grant, K.M., 2015. Mediterranean climate and oceanography, and the periodic development of anoxic events (sapropels). Earth Sci. Rev. 143, 62–97.
Sabatier, P., Dezileau, L., Colin, C., Briqueu, L., Bouchette, F., Martinez, P., Von Grafenstein, U., 2012. 7000 years of paleostorm activity in the NW Mediterranean Sea in response to Holocene climate events. Quaternary Research 77 (1), 1–11.
Santacroce, R., Cioni, R., Marianelli, P., Sbrana, A., Sulpizio, R., Zanchetta, G., Joron, J. L., 2008. Age and whole rock–glass compositions of proximal pyroclastics from the major explosive eruptions of Somma-Vesuvius: A review as a tool for distal tephrostratigraphy. Journal of Volcanology and Geothermal Research 177 (1), 1–18.
Schilman, B., Bar-Matthews, M., Almogi-Labin, A., Luz, B., 2001. Global climate instability reflected by Eastern Mediterranean marine records during the late Holocene. Palaeogeogr. Palaeoclimatol. Palaeoecol. 176 (1–4), 157–176.
Schmiedl, G., Mackensen, A., Müller, P.J., 1997. Recent benthic foraminifera from the eastern South Atlantic Ocean: Dependence on food supply and water masses. Mar. Micropaleontol. 32, 249–287.
Sgarrella, F., Moncharmont-Zei, M., 1993. Benthic Foraminifera of the Gulf of Naples (Italy): systematics and autoecology. Boll. Soc. Paleontol. It. 32, 145–264.
Sparnocchia, S., Gasparini, G.P., Astraldi, M., Borghini, M., Pistek, P., 1999. Dynamics and mixing of the Eastern Mediterranean outflow in the Tyrrhenian basin. J. Mar. Syst. 20 (1–4), 301–317.
Stow, D.A.V., 1977. Late Quaternary Stratigraphy and Sedimentation on the Nova Scotian Outer Continental Margin. Unpublished Ph.D. Thesis. Dalhousie University, Halifax, NS, 360 pp.
Stow, D.A.V., Faugeres, J.-C., 2008. Contourite facies and facies model. In: Contourites, M. Rebesco, Camerlenghi, A. (Eds.), Developments in Sedimentology, 60. Elsevier, pp. 223–250.
Stow, D., Smillie, Z., 2020. Distinguishing between deep-water sediment facies: turbidites, Contourites and Hemipelagites. Geosciences 10 (2), 68.
Stow, D.A.V., Pudsey, C.J., Howe, J.A., Faugères, J.-C., Viana, A.R., 2002a. Deep-water contourite systems: modern drifts and ancient series, seismic and sedimentary characteristics. Geol. Soc. Lond. Mem. 22.
Stow, D.A., Faugères, J.C., Gonthier, E., Cremer, M., Llave, E., Hernández-Molina, F.J., Diaz-Del-Rio, V., 2002b. Faro-Albufeira drift complex, northern Gulf of Cadiz. Geol. Soc. Lond. Mem. 22 (1), 137–154.
Stow, D.A.V., Faugeres, J.-C., Howe, J., Pudsey, C., Viana, A., 2002c. Bottom currents, contourites and deep sea sediment drifts: current state-of-the-art. In: Stow, D., Pudsey, C., Howe, J., Faugeres, J.-C., Viana, A. (Eds.), Deep-Water Contourite Systems: Modern Drifts and Ancient Series, Seismic and Sedimentary Characteristics. Geological Society Memoirs, London, pp. 7–20.
Tanguy, J.C., Le Goff, M., Principe, C., Arrighi, S., Chillemi, V., Paiotti, A., La Delfa, S., Patanè, G., 2003. Archeomagnetic dating of Mediterranean volcanics of the last 2100 years: validity and limits. Earth and Planet. Sci. Lett. 211 (1-2), 111–124.
Thiéblemont, A., Hernández-Molina, F.J., Miramontes, E., Raisson, F., Penven, P., 2019. Contourite depositional systems along the Mozambique Channel: the interplay between bottom currents and sedimentary processes. Deep Sea Res. Part I 147, 79–99.
Thunell, R.C., Reynolds, L., 1984. Sedimentation of planktonic foraminifera: Seasonal changes in species flux in the Panama Basin. Micropaleontology 30, 243–262.
Toucanne, S., Mulder, T., Schönfeld, J., Hanquiez, V., Gonthier, E., Zaragosi, S., 2007. Contourites of the Gulf of Cadiz: a high-resolution record of the paleocirculation of the Mediterranean outflow water during the last 50,000 years. Palaeogeography, Palaeoclimatology, Palaeoecology 246 (2-4), 354–366.
Toucanne, S., Jouet, G., Ducassou, E., et al., 2012. A 130,000-year record of Levantine Intermediate Water flow variability in the Corsica Trough, western Mediterranean Sea. Quat. Sci. Rev. 33, 55–73.
Tripsanas, E.K., Panagiotopoulos, I.P., Lykousis, V., Morfis, I., Karageorgis, A.P., Anastasakis, G., Kontogonis, G., 2016. Late quaternary bottom-current activity in the south Aegean Sea reflecting climate-driven dense-water production. Mar. Geol. 375, 99–119.
Vallefuoco, M., Lirer, F., Ferraro, L., Pelosi, N., Capotondi, L., Sprovieri, M., Incarbona, A., 2012. Climatic variability and anthropogenic signatures in the Gulf of

Salerno (southerneastern Tyrrhenian Sea) during the last half millennium. Rend. Fisici Accad. Lincei 23, 13–23.
Viana, A.R., De Almeida, W., De Almeida, C.W., 2002. Upper slope sands: late Quaternary shallow-water sandy contourities of Campos Basin, SW Atlantic Margin. Geol. Soc. Lond. Mem. 22 (1), 261–270.
Voelker, A.H.L., Lebreiro, S.M., Schonfeld, J., Cacho, I., Erlenkeuser, H., Abrantes, F., 2006. Mediterranean outflow strengthening during northern hemisphere coolings: a salt source for the glacial Atlantic? Earth Planet. Sci. Lett. 245, 39–55.
Yin, S., Hernández-Molina, F.J., Zhang, W., Li, J., Wang, L., Ding, W., Ding, W., 2019. The influence of oceanographic processes on contourite features: a multidisciplinary study of the northern South China Sea. Mar. Geol. 415, 105967.
Zanchetta, G., Sulpizio, R., Roberts, N., Cioni, R., Eastwood, W.J., Siani, G., Santacroce, R., 2011. Tephrostratigraphy, chronology and climatic events of the Mediterranean basin during the Holocene: an overview. The Holocene 21 (1), 33–52.
Zarries, M., Mackensen, A., 2010. The tropical rainbelt and productivity changes off northwest Africa: a 31,000-year high-resolution record. Mar. Micropaleontol. 76, 76–91.